Spectroscopic and Computational Studies of the Hydrogen Bonding Interactions of Hydroxyethyl Ethers

By: Ashley Williams

A thesis submitted to the faculty of The University of Mississippi in partial fulfillment of the requirements of the Sally McDonnell Barksdale Honors College.

Oxford, MS
May 2017

Approved by:

Dr. Nathan I. Hammer
Advisor

Dr. Steven R. Davis
Reader

Dr. John Samonds
Reader

Acknowledgements

The University of Mississippi has blessed me with opportunities I would have never thought possible upon embarking on my college journey. The countless people who have mentored me and helped ensure my success is astounding. First I would like to thank Dr. Nathan Hammer for his consistent faith in me, and his insistence that I do not quit when things get hard. His guidance and wisdom have been paramount in making me both the student and person that I am today. The Ole Miss Women's Council has also been integral in facilitating my success at Ole Miss, as they provided me with weekly guidance and a home away from home, as well as a leg up in my academic and career goals with interview practices, resume-building sessions, and leadership conferences. I would like to thank my lab group, the Hammer group, particularly Shane Autry and Louis McNamara, for their constant source of knowledge and help constructing my matrix isolation Raman spectrometer. Finally, I would like to thank my parents, Suzy and Wayne Williams, and my sister, Anna Katherine Williams, for the tremendous amount of support, love, and encouragement over the years.

Spectroscopic and Computational Studies of the Hydrogen Bonding Interactions of Hydroxyethyl Ethers

Ashley E. Williams (under the direction of Dr. Nathan Hammer)

The isoenzymatic form of microsomal cytochrome P450, CYP2E1, is involved in the formation of oxygen free radicals, specifically hydroxyethyl ether. Chronic alcohol abuse has been found to induce larger levels of CYP2E1 in the liver, thus increasing production of these harmful free radicals. Generation of the hydroxyethyl ether oxygen free radicals occurs during the metabolism of ethanol in microsomes. The hydrogen-bonding interactions of hydroxyethyl ethers with water have yet to be analyzed, and information regarding the interactions with water can be applied directly to biological systems. Here, we employ Raman spectroscopy and computational chemistry to study hydroxyethyl ether complexes in micro-solvated networks of varying complexity.

Table of Contents

Copyright Page

Acknowledgements

Abstract

Chapter 1: Chemical Bonds and the Human Body.....1

1A. Ionic Bonds.....1

1B. Covalent Bonds.....2
…….Nonpolar and Polar Covalent Bonds

1C. Hydrogen Bonds.....3
…….Definition of Hydrogen Bonds
…….1-Hydroxyethyl Radical

Chapter 2: Spectroscopy.....5

2A. What is spectroscopy?.....5
……Definition of Spectroscopy and the Electromagnetic Spectrum
……Colors and Corresponding Wavelengths
……Types of Spectroscopy and Common Uses

2B. Vibrational Spectroscopy.....8
……Harmonic Oscillator

2C. Raman Spectroscopy.....12
……What is Raman Spectroscopy?
……Vibrations
.....Analyzing Spectra

2D. Instrumentation.....18
…… Raman Spectrometer

Chapter 3: Theory.....21

3A. Potential Energy Surfaces.....21
……Hartree-Fock Molecular Orbital Theory
……Density Functional Theory
……Optimization and Frequency Calculations

3B. Method and Basis Set.....27
……UB3LYP
……6-31++G(*d,p*)
……aug-cc-pVTZ

Chapter 4: Experimental Outline and Theoretical Results.....29

4A. Experimental Setup.....29
…….Matrix Isolation Raman Spectrometer
…….Experimental Reaction Overview

4B. Results: Lowest-Energy Structures.....32
…….Lowest-Energy Structures Listed
…….Calculated Water Molecule Binding Energies
…….Lowest-Energy Structures and Theoretical Raman Spectra
…….Shifting
…….Vibrational Modes
.....Discussion

Chapter 5: Conclusions & Future Work.....59

References.....60

Chapter 1: Chemical Bonds and the Human Body

Chemical bonds play an important role in the human body. The unique bonds that can form between atoms contribute to the overall structure and stability of molecules as well as to interactions with their surroundings. In biology, this fact is no different, and the different bonding mechanisms are important in many fundamental biological processes including the electron transport chain and glycolysis.

1A: Ionic Bonds

Ionic bonds occur between a metal and a nonmetal, and result in a permanent gain or loss of an electron. There is generally a large difference in electronegativity between the two participating atoms. This transfer stabilizes the two atoms because the shared electron/s might fill a nearly filled subshell of one of the atoms, and empty the unstable single valence electron in a subshell of the other atom, revealing the next completely full and stable valence subshell. Ionic bonds are quite prevalent in the human body, and a good example is sodium chloride, NaCl. Sodium has one valence electron in the 3s subshell, while Chloride has seven electrons in its 3p subshell. Chloride is very electronegative, with a small effective nuclear charge, so the chloride atom easily takes sodium's single valence electron, forming two ions with opposing and attracting charges and creating an ionic bond, stabilizing both participating atoms.

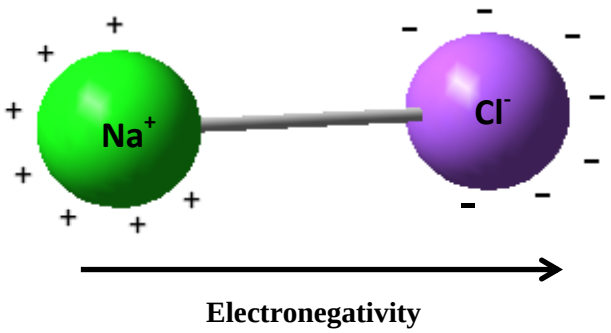

Figure 1.1: Cl^- is strongly electronegative, so it pulls the electrons from Na^+, leaving a partial positive charge on the sodium atom and a partial negative charge on the chloride atom.

1B: Covalent Bonds

Covalent bonds characteristically involve the sharing of electrons, as opposed to the permanent transaction of ionic bonding. Covalent bonds often occur when a nonmetal binds to another nonmetal, both in search of electrons to fill their valence subshells. The interaction of sharing electrons lowers the potential energy of the two nuclei because of stabilization due to electrostatic interactions, and the electrons are shared to fill the valence shells of both atoms[17]. There are two different types of covalent bonds, depending on the types of atoms interacting. In a nonpolar covalent bond, the sharing of the electron's negative charge is equal, as is the positive electrical pull of the protons inside the nucleus[16]. Basically, nonpolar covalent bonds form between molecules that are electrically balanced. However, if there are regions containing opposing charges in the same atom, or more positive or negative charge is pulled towards one of the atoms, a polar covalent bond forms. A good example of this in biology can be seen in the electron

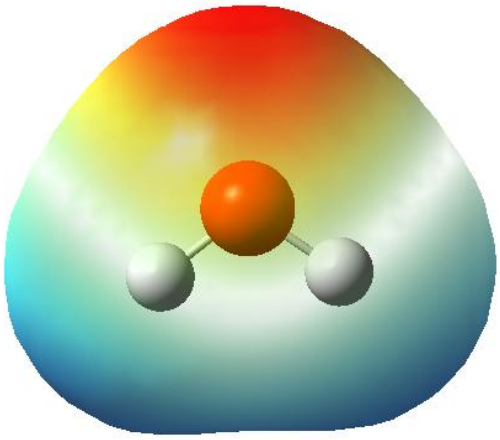

Figure 1.2: Electron density diagram of a water molecule. Optimized using Hartree-Fock method and 3-21 G basis set. Diagram created in Gaussian.

density diagram of a water molecule (Figure 1.2). The oxygen atom is strongly electronegative, and pulls more of the electron's negative charge towards itself in the center of the molecule (the red area signifies the negative charge near the oxygen atom in the center), leaving the hydrogen atoms with a partial positive charge. This partial positive charge creates the possibility for our final bonding type: hydrogen bonds.

1C: Hydrogen Bonds

Hydrogen bonds form when a hydrogen atom is bound to a molecule that is pulling electron density away, leaving a partial positive charge on the hydrogen atom. A nearby electronegative atom can interact and bond with this partially positive hydrogen atom, forming a micro-solvated network of water molecules. Hydrogen bonds are much stronger than other dipole-dipole interactions because the one electron from the hydrogen atom is primarily located in the O-H bond. This reduces Pauli repulsion, allowing the hydrogen molecules to get extremely close to the electronegative atoms of other molecules. This can also be seen in the interaction of a water molecule with other water

molecules, contributing to many of the characteristics of water commonly observed in nature including surface tension and adhesion.

Hydrogen bonding is an important molecular phenomenon occurring at the most basic level of chemistry in the human body. In the study of the liver and alcohol-related injuries and deaths, a specific radical formed during ethanol metaolism is specifically toxic and consistent, high levels of this radical have been related to cirrhosis of the liver, liver cancers, and other alcohol-related liver diseases. An ethanol-inducible enzyme,

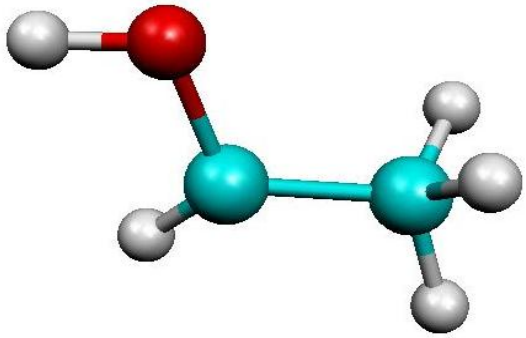

Figure 1.3: Structure of 1-Hydroxyethyl Radical

cytochrome p450, specifically the mutated form of this protein, CYP2E1, generates reactive oxygen species when breaking down ethanol in the body. Ethanol is reduced to the toxic chemical, acetaldehyde, which is further broken into superoxide radicals and hydrogen peroxide. These molecules react and subsequently lead to the formation of the toxic radical, 1-Hydroxyethyl radical (see Figure 3). This radical can also be produced via direct catalysis by stealing a hydrogen atom from ethanol at the active site of CYP2E1. Understanding the relationship between the 1-Hydroxyethyl radical and water molecules provides us with a more thorough understanding of this unstable radical's nanomolecular interactions.

Chapter 2: Spectroscopy

2A: What is Spectroscopy?

Definition of Spectroscopy and Electromagnetic Spectrum

Spectroscopy is the study of light-matter interactions. Molecules have characteristic values for processes such as absorption and emission, and this information can be used by a variety of different instruments to determine the identity of an unknown, determine the presence of different elements in a sample, etc. Light is electromagnetic radiation, an energy that is made up of oscillating electric and magnetic fields[17]. Photons are particles of light, and these principles operate under the assumption that light propagates in space. This happens to photons on the entire spectrum, not just in the visible regions, so the applications of spectroscopy are vast. A spectrum was created to compare the different types of radiation, and their different wavelengths and corresponding different energy. The longer the wavelength of a wave, the lower the energy of that wave, and vice versa. This is also seen with the frequency of a wave. As the wavelength increases, the frequency of the wave decreases.

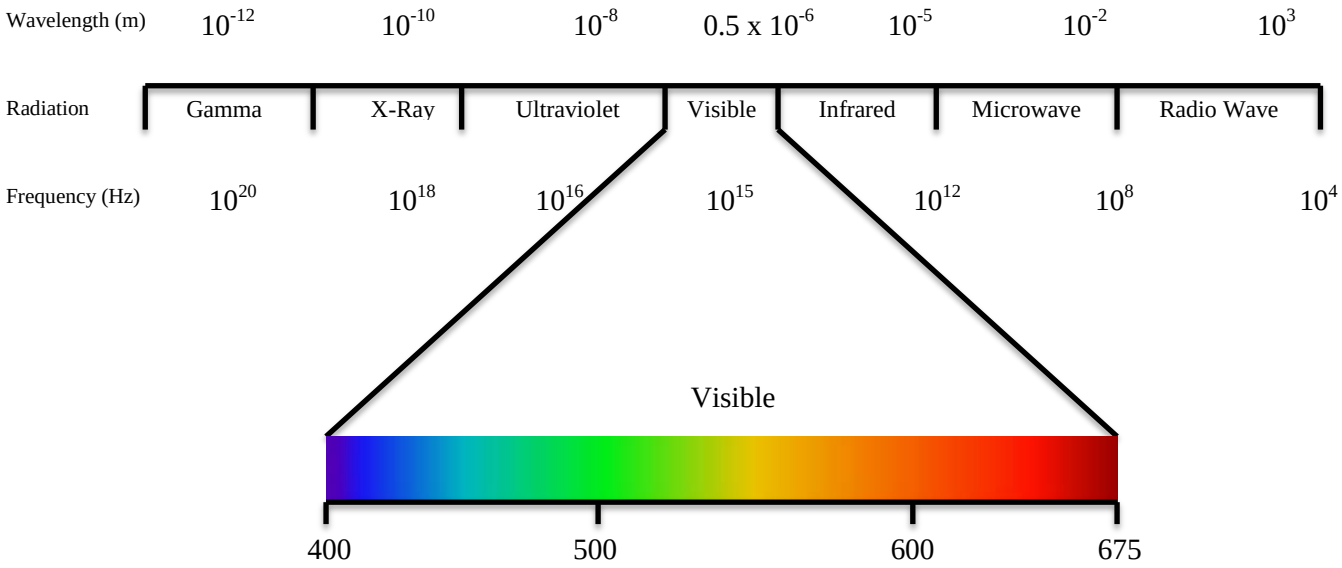

Figure 2.1: Electromagnetic Spectrum and close-up view of the visible region of the spectrum.

Color	Wavelength (λ)
Red	650 nm
Orange	590 nm
Yellow	570 nm
Green	510 nm
Blue	475 nm
Violet	400 nm

Table 2.1: Colors of the visible region of the electromagnetic spectrum and their corresponding wavelengths.

Types of Spectroscopy and Common Uses

Nuclear Magnetic Resonance Spectroscopy works under the principle that the magnetic nuclei in a magnetic field absorb and re-emit radiation. This type of molecular spectroscopy is not destructive to the sample and is a qualitative measurement used for structural determination via the number, type (singlet, doublet, triplet), and position of protons and carbon atoms[9] that appear on the produced spectrum.

Infrared Spectroscopy occurs when absorption of energy leads to vibrational energy transitions, and relies on the concept that the vibrations cause a shift in the dipole moment of the molecule being studied. This method of molecular spectroscopy is not destructive to the sample and is a qualitative measurement used to identify different functional groups in a molecule[9].

Raman Spectroscopy occurs when absorption of light results in inelastic scattering of monochromatic light, and this results in energy shifts that give information of vibrational modes. This instrument is commonly used in accordance with Infrared Spectroscopy, and is used for fingerprinting molecules, and observation of changes in bonding[9].

UV-Vis Spectroscopy is a type of molecular spectroscopy that occurs when absorption due to electronic transitions with weakly held electrons takes place and is often used to investigate the functional groups and molecules with unsaturated bonds[9].

Mass Spectroscopy is a type of elemental analysis that separates and detects ions based on their mass to charge ratio, m/z. There are a number of different techniques employed in mass spectrometers, for example, Time of Flight Mass spectrometry. This is a

destructive method of instrumentation, but it is commonly employed in determining the concentration of multiple elements and isotope ratios at ultra-trace levels. Knowing the mass of the molecule being studied can often allude to its identity[9].

Chromatography is a method of separation used to prepare samples for many spectroscopic methods. There are several different types of chromatography including gas chromatography, ion chromatography (ion-exchange), and liquid chromatography, which all work basically by differential partitioning into the stationary phase in the column[9].

2B: <u>Vibrational Spectroscopy</u>

Spectroscopy relies heavily upon the understanding that when light encounters a molecule in the ground energy state, the photon will be absorbed, causing electrons bound to the molecule to become energetically excited and jump to some excited state. The excited electrons are assumed to eventually regain equilibrium and return to the ground state. This emission can be either spontaneous or stimulated. Spontaneous emission is the most common, and can occur via two pathways, fluorescence, or phosphorescence. In fluorescence, the electrons have the same spin state multiplicity, whereas in phosphorescence, the electrons have different spin state multiplicities.

Spectroscopy simply measures intensity of a response (a peak), versus the frequency of the light that causes the response. The intensity corresponds to a measure of the rate of transitions taking place between the ground and some excited states, and the frequency is

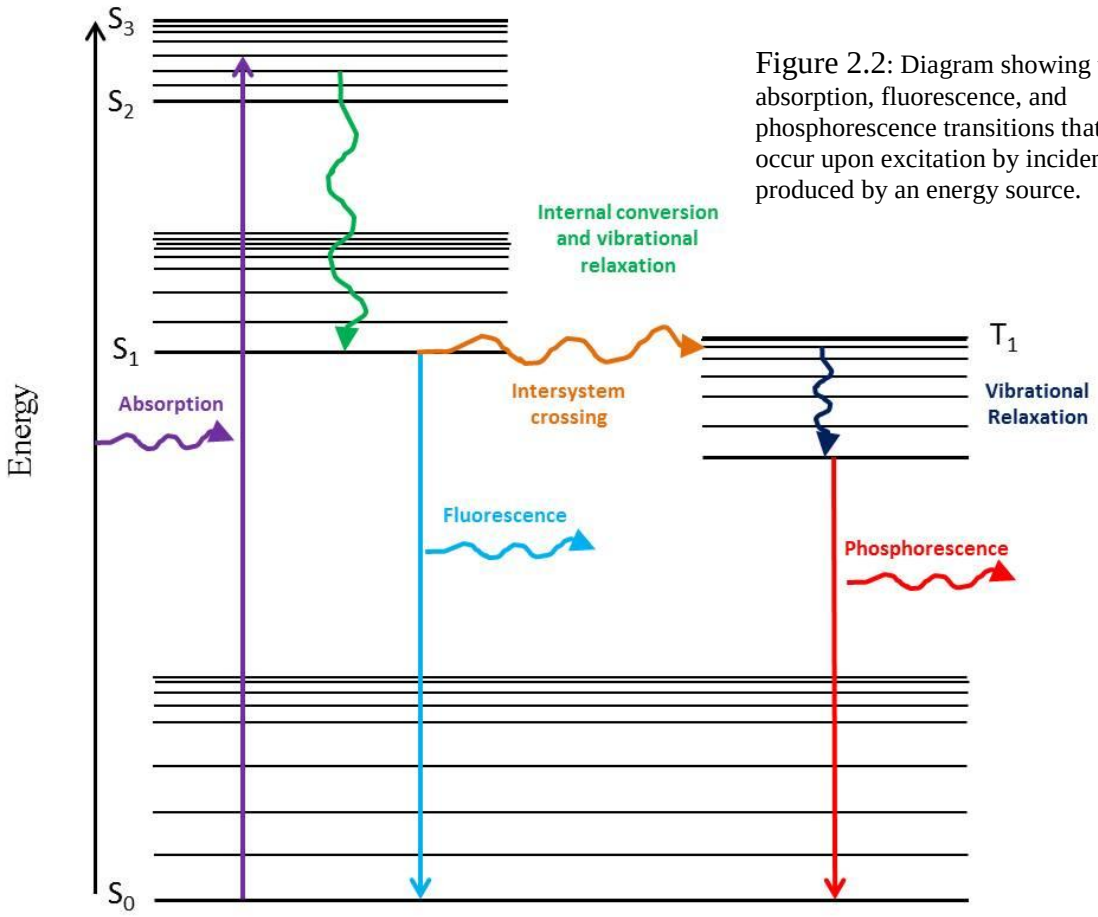

Figure 2.2: Diagram showing the absorption, fluorescence, and phosphorescence transitions that can occur upon excitation by incident light produced by an energy source.

a measurement of the difference in energy between the ground and excited states (the difference in energy before and after an electron becomes excited).

Quantum chemistry categorizes four primary types of transitions possible during an excitation, and they are translational, rotational, vibrational, and electronic. The different types of radiation on the electromagnetic spectrum can be differentiated by the type of transitions that occur in each. For example, infrared rays consist of heat radiation that cause vibrational transitions, microwaves cause rotational transitions, and ultraviolet rays cause electronic transitions. The order of the size of the transitions is as follows: Translational < Rotational < Vibrational < Electronic. Understanding this trend, one

can see why the higher energy UV-vis radiation causes the largest electronic transitions, whereas the lower energy microwaves cause rotational transitions.

The Harmonic Oscillator

For the purpose of this experiment, we will focus on vibrational transitions. Vibrational transitions are modeled by the harmonic oscillator and can be explained with both classical physics and quantum theory. In classical physics, considering a spring attached to mass, *m*, being held stationary, it can be assumed that under Hooke's law, the force on the spring is proportional to the displacement of the mass: $F = -kx$. Considering the motion of a spring, first it moves outward and then immediately returns, although not fully, back to its initial position. This return flight is represented by a negative sign and is called the restoring force. *k* is the force constant and is a measure of the rigidity of the spring. The force can also be related to the potential energy by the equation $F = -dV/dx \rightarrow V= (1/2)kx^2$. V is called the harmonic potential, standing for the spring being stretched out infinitely far and then springing infinitely back in the other direction. This equation is that of a parabola, and if considered using only very small displacements, it is a good approximation for harmonic oscillation of electrons[12].

In the classical physics explanation, consider a mass with a pen attached to a spring undergoing constant motion and no friction. The wave being recorded on a graph of position vs. time could thus be either sine or cosine. The amplitude (maximum displacement), x_0, can be found from the initial settings of the oscillation, and the natural frequency of the oscillator has previously been discovered to be $\sqrt{\frac{k}{m}}$. According to this theory, the more rigid a spring and the lighter the masses, the higher frequency the wave.

An important difference in the classical physics explanation is the amplitude of the wave can be anything, any energy, and this is quite different from that in the quantum mechanical harmonic oscillator.

In the quantum mechanical harmonic oscillator model, we think of a different picture. Consider two masses held together by a Hooke's law spring. The displacement of the spring from its initial location, R, and returning to its equilibrium location, R_e, can be shown as $x = R - R_e$. If we input this equation into our Hamiltonian, the equation becomes:

$$\hat{H} = \frac{-\hbar}{2\mu}\frac{d^2}{dx^2} + \frac{1}{2}kx^2$$

The eigenvalues of the harmonic oscillator Hamiltonian correspond to the energy levels of the harmonic oscillator and appear as straight horizontal lines in the harmonic oscillator model.

$$E_v = \left(v + \frac{1}{2}\right)hv_0$$

-where the quantum numbers $v_0 = 0, 1, 2, ...\infty$

For this specific problem, with the two masses attached at either end of a spring, there is only one quantum number and the energy levels are non-degenerate, allowing us to solve for v_0:

$$v_0 = \frac{1}{2\pi}\sqrt{\frac{k}{\mu}}$$

We are also able to find that the position-momentum uncertainty principle results in zero-point energy[12].

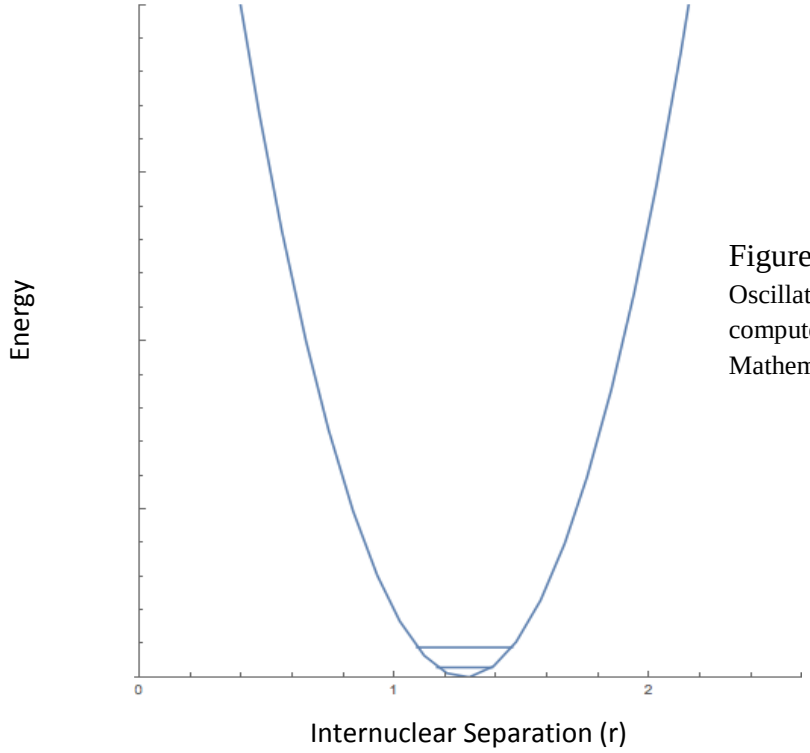

Figure 2.3: Harmonic Oscillator, graphed in the computer program Mathematica.

2C: Raman Spectroscopy

What is Raman Spectroscopy?

Raman Spectroscopy is a type of spectroscopy that involves the vibrational transitions of electrons, as modeled before by the explanation of the harmonic oscillator. However, unlike other methods of spectroscopy that are based on absorption of radiation, such as IR, UV-Vis, and NMR, Raman spectroscopy focuses on detecting the scattering of radiation. In order for a molecule to be Raman-active, there must be a change in polarizability in the molecule. Polarizability can be described in the effect that an electric field has on a molecule, as the electron distribution can be changed depending on the molecule and motion caused by a transition. This polarizability must be directionally

dependent, or anisotropic, for a molecule to be Raman-active. When a molecule has more electrons, the nuclear charge has less control on charge distribution, and the polarizability is seen to increase. When the electrons move farther away from the nucleus, the polarizability also increases, so distortion of the electric distribution is easier as bond lengths increase and harder as bond lengths decrease. To determine whether a molecule is Raman active, one must determine whether or not a molecule is polarizable. A vibrational mode is produced by the change in polarizability. For example, let us consider O = C = O. Symmetric stretching of this molecule is not Raman-active because the motion of the stretch is simultaneous and the polarizability cancels. However, an asymmetric stretch of this molecule is Raman-active because the O bonds alternate stretching.

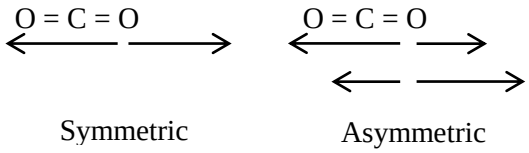

The scattering of light can take place in three ways: Rayleigh scattering, Stokes scattering, and Anti-Stokes scattering. Basic scattering of light occurs when a photon interacts with a molecule and a transfer of energy occurs between the two atoms, either a gain or loss, and excite the molecule to a virtual "excited" state. A molecule with a time-dependent electric field and characteristic vibrational frequency is given by the equation:

$$E = E_0 cos(2\pi\nu t)$$

The negatively charged valence electrons and positively charged nucleus interact with the electric field and cause distortion in the molecule because of the opposing forces of the electrons and positive nucleus. This distortion results in a time-dependent dipole moment, $\mu_{induced}(t)$, which is the same frequency as the electric field. The dipole moment and

electric field magnitude are linearly proportional and the proportionality constant is the polarizability, α. The proportionality constant, or polarizability, α, is dependent on the electric field's direction relative to the molecule and its axes[12].

$$\mu_{induced}(t) = \alpha E_0 cos(2\pi vt)$$

Because polarizability is basically a measure of distortion based on movement of electron distribution in a molecule relative to its interaction with an electric field of a specific direction, it also relies heavily on the bond length of a molecule, $x_e + x(t)$, where x_e is known as the equilibrium value. A Taylor-Maclaurin series can be employed so that the terms after the first order are able to be neglected.

$$\alpha(x_e + x) = \alpha(x_e) + x(\frac{d\alpha}{dx})_{x=x_e} + \cdots$$

The vibration of the molecule can be described as time dependent:

$$x(t) = x_{max} cos(2\pi v_{vib} t)$$

Once we have combined the previous two equations we arrive to[12]:

$$\mu_{induced}(t) = \alpha E = E_0 \cos(2\pi vt) \left[\alpha(x_e + \left\{\left(\frac{d\alpha}{dx}\right)_{x=x_e}\right\} x_{max} \cos(2\pi v_{vib} t)\right]$$

Using trig identities, this can be further simplified to:

$$\mu_{induced}(t) = \alpha E$$

$$= \alpha(x_e)E_0\cos(2\pi\nu t) + \left[\left(\frac{d\alpha}{dx}\right)_{x=x_e}\right]x_{max}E_0[\cos\{2\pi(\nu + \nu_{vib})t\}$$

$$+ \cos\{2\pi(\nu - \nu_{vib})t\}]$$

The three frequencies, ν, (ν-ν_{vib}), and (ν+ν_{vib}) are radiated light by the time-varying dipole moment and correspond to Rayleigh, Stokes, and Anti-Stokes frequencies, respectively. In order for a Stokes or Anti-Stokes transition, $\frac{d\alpha}{dx} \neq 0$, or the polarizability cannot be zero and must change in order for a molecule to be Raman-active. Below is a figure showing the different types of scattering that can occur[12].

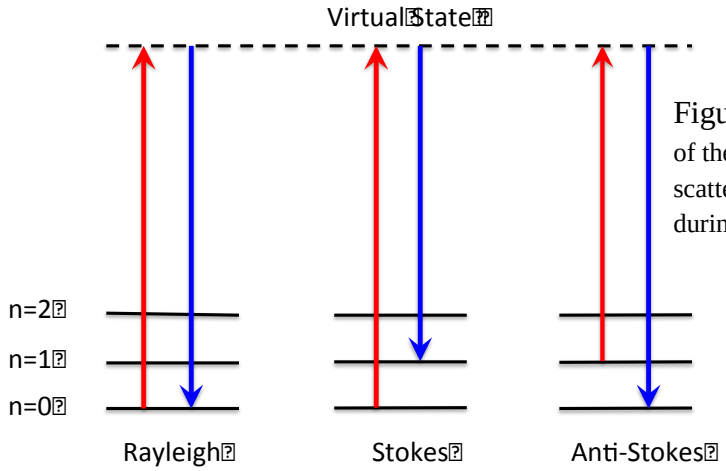

Figure 2.4: Depiction of the different types of scattering that can occur during a Raman event.

It is important to note that $\frac{d\alpha}{dx}$ is the change in polarizability in diatomic molecules. In order to compensate for more atoms, $\frac{d\alpha}{dq}$ is used to define the change in polarizability in polyatomic molecules. Instead of thinking of the photon as being absorbed, it is better to consider the photons exciting the molecule to a higher energy "state" which is ephemeral. The initial and final states are eigenfunctions of the time-dependent Schrodinger equation, but this higher excited state does not have to follow this requirement, which is why it is referred to as the virtual state.

Vibrations

Vibrational excitation can lead to several different types of vibrational motions. The two most broad categories include stretching and bending. Stretching vibrations consist of symmetric and asymmetric stretching, or motions that change the length of the bonds. Bending vibrations consist of wagging, twisting, rocking, and scissoring, and correspond to motions that change the bond angle of the molecule.

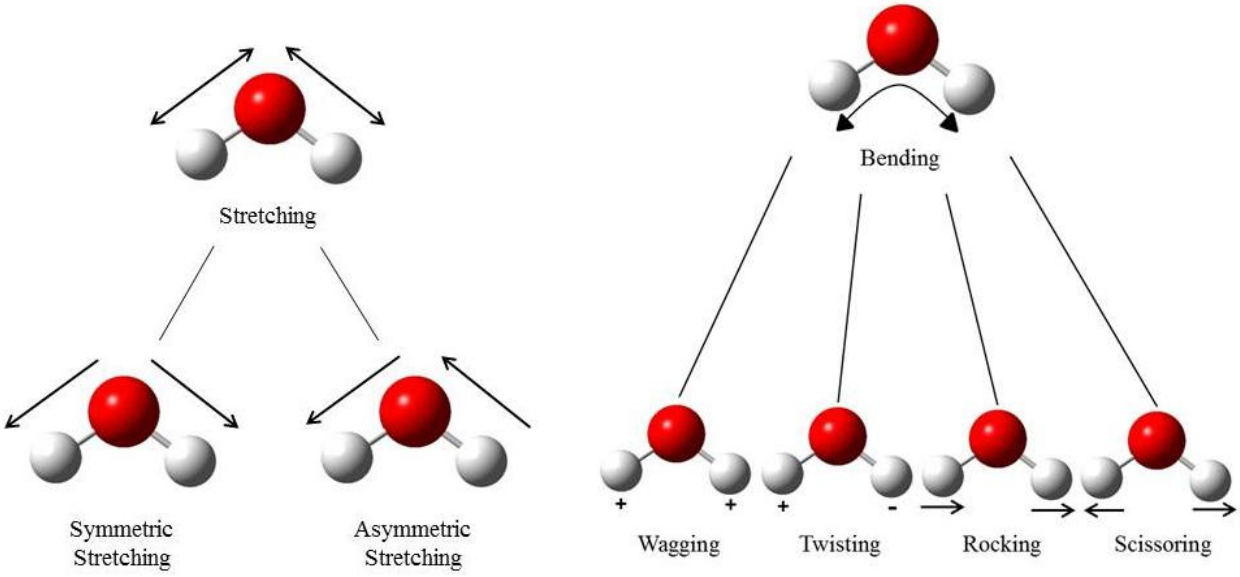

Figure 2.5: Some of the vibrational motions possible with Raman spectroscopy.

Symmetric stretching modes are more commonly seen in Raman spectroscopy than asymmetric stretching modes, because in order for a vibrational motion to be Raman-active, there must be a change in the polarizability of the molecule. Symmetric stretching increases and decreases the distance between the electron clouds of the atoms involved in the stretch, thus increasing and decreasing the polarizability of the molecule as a whole. Asymmetric stretching results in cancelling of the changes in polarizability because the

change is equally opposite. Bending vibrational modes are also not as commonly seen in Raman spectroscopy; however, they are often strongly seen in IR spectroscopy.

Analyzing Spectra

Raman spectroscopy is commonly used to fingerprint molecules, as well as to identify the different types of functional groups that are present in the model and to detect changes in bonding. It is commonly used in accordance with IR analysis, as the group frequencies of functional groups fall in roughly the same regions as in IR spectroscopy. In the Hammer Group, Raman spectroscopy is commonly used to detect hydrogen-bonding interactions between molecules of water or another solvent and the sample. The H-H vibrational bond frequency can be found around ~4401 cm^{-1}.

Remember that Raman scattering is an inelastic process, so the scattered light does not have the same frequency as the incident light. Instead, there is a transfer of energy that occurs which corresponds to the vibrational energy transitions upon excitation. If the sample molecules gain energy from the incident light, this is referred to as Stokes Raman scattering; if the sample molecules lose energy to the incident light, this is referred to as Anti-Stokes Raman scattering. The scattered light is measured and Stokes and Anti-Stokes lines can be seen in Raman spectra. Anti-Stokes lines are much less intense than Stokes lines. These lines are also seen to shift in the spectra. Stokes scattered lines red shift to a longer wavelength (lower energy), whereas anti-Stokes scattered lines blue shift to a shorter wavelength (higher energy) in the spectra. (See Figure 2.4). The shifting that is seen in specific Raman spectra can be correlated to the changes in bonding in the molecule.

2D: Instrumentation

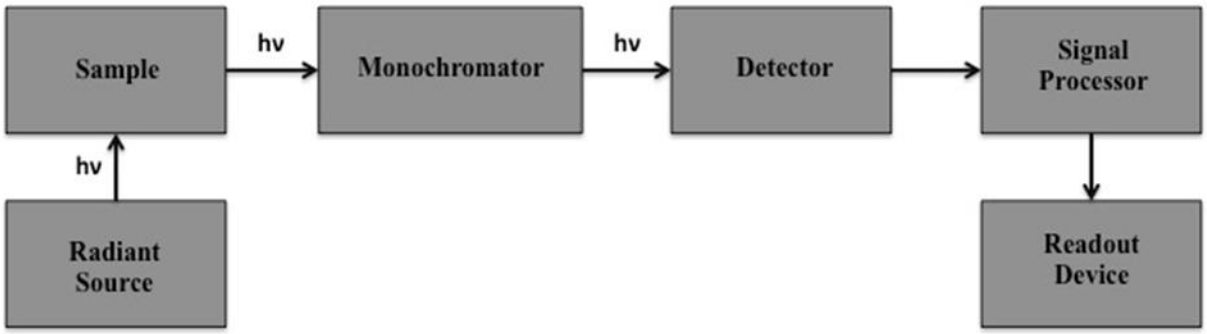

Figure 2.6: Basic instrumentation schemata of a Raman spectrometer.

Shown in Figure 2.6 is a basic schemata of a Raman spectrometer. The radiant sources commonly used in Raman spectroscopy are lasers. A population inversion is responsible for the energy produced by lasers, and this is basically just the electrocution of a specific molecule: excitation via electricity. A laser cavity consists of a pumping source, high reflector (rear mirror), output coupler, and prism. A laser is chosen because it ensures high resolution and is more discreet. There are four important characteristics of laser lines: coherency monochromatic, polarizable, and collimating. Lasers are coherent in that wavelengths at any point in the beam are in-phase. They consist of a single wavelength, and thus are monochromatic. They are polarizable, meaning the wave oscillates in a single plane, and finally, they are collimating, in that lasers consist of thin, intense beams with little to no divergence[12].

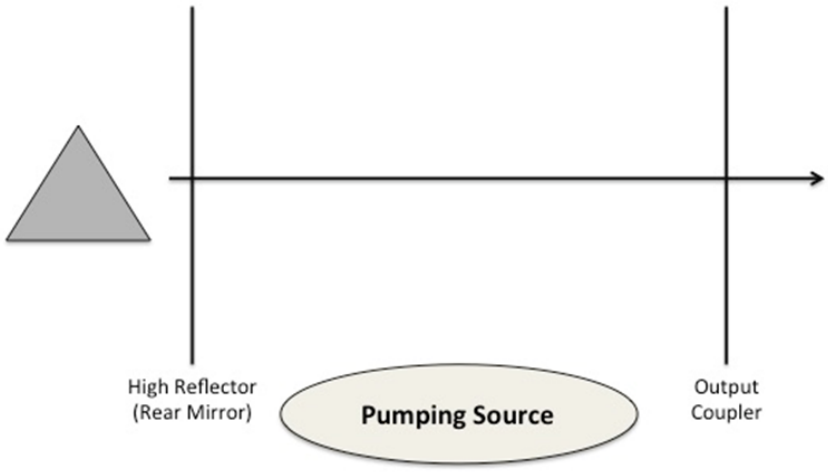

Figure 2.7: Example of a laser cavity seen as the excitation source for many different types of spectroscopy.

Excitation by the laser causes the scattering of light. The transmission of energy between the incident light and the sample molecules results in the vibrational transitions that are seen in Raman spectroscopy. The vibrational transitions correspond to vibrational motions in which there is a change in the polarizability of the molecule. There are a number of motions that can be elicited from excitation, most commonly stretching and bending (see Figure 2.5). The most common lasers used for Raman spectroscopy are listed in Table 2.2. New laser sources have been researched, and are now also commonly employed in Raman spectroscopy, such as diode lasers.

Laser	**Wavelength, λ**
Ruby laser	694.3 nm
HeNe	632.8 nm
CO_2	10.6 μm
N_2	337.1 nm (UV)
Ar^+/Kr^+	457, 488, 514 nm

Table 2.2:Common lasers used in Raman spectroscopy and their corresponding wavelengths.

The most common detector used in Raman spectroscopy today is a charge-coupled device (CCD) detector. Other detectors that can be used include photomultiplier tubes and array detectors. A silicon CCD works with a grating, which discriminates between specific wavelengths. The grating selects the specific wavelength that will hit the pixels on the CCD detector. The detector is heat-sensitive, so cooling the detector surface can decrease the thermal noise from the detector, thus increasing the signal-to-noise ratio[9]. The CCD commonly detects wavelengths between 400 and 1,000 nm[9].

Chapter 3: Theory

3A: Potential Energy Surfaces

Most experimental chemists rely on theoretical chemistry to confirm experimental findings. Theoretical chemistry encompasses a broad range of programs and approximation techniques and has created the possibility to study highly reactive, never-before-synthesized molecules and compounds, as well as to observe several characteristics of molecules including molecular structure, determination of lowest-energy structures, vibrational stretching modes expected when undergoing Raman spectroscopy, etc. The technological revolution and increasing capabilities of computer software and programming have made it possible to account for many aspects of chemical reactions and experimental chemistry, and combining them together has provided experimental chemists an outlet with which to compare their work.

In the curriculum for most general chemistry courses, a basic chemical reaction mechanism is explained and compared to a graph. The graph provides information regarding the reaction coordinate and how it corresponds with energy changes. Different energy states of molecules correspond to different energy. Reactants are generally stable, low-energy molecules, as are products; however, they end up at a different energy than the reactants began with. In between these two states is a

higher-energy, unstable transition state. On a reaction coordinate diagram, we can see this oscillation as reactions begin at low energy and increase during the transition state and then fall back down to lower energy in product form[17].

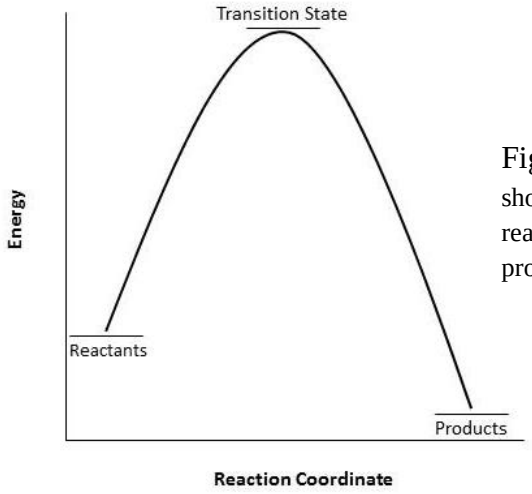

Figure 3.1: Reaction coordinate showing the relative energies of the reactants, transition state, and products of a reaction.

The purpose of these explanations is to show the equilibrium found in stable molecular structures, which are at energy minima, versus the instability and resulting higher energy that a molecule feels when in this transition state, found at energy maxima. An important aspect of computational chemistry is the use of quantum chemistry software to make necessary approximations to solve the Schrodinger equation, which provides the lowest-energy molecular structure that could theoretically exist during a chemical reaction. The reaction coordinate can also be used to explain the vibrational modes seen in molecules using experimental methods such as Raman spectroscopy[7]. Each stretch found in an optimization of a complex is a motion of that molecule away from its equilibrium structure, showing the continual oscillation of molecules from equilibrium to non-equilibrium and back to equilibrium. The point is that observing the movement of

vibrational modes is viewing the molecule oscillate back-and-forth near equilibrium, trying to settle in the lowest energy, most-stable state[7].

Hartree-Fock Molecular Orbital Theory

As mentioned before, it is impossible to solve the Schrodinger equation for multi-atom systems. However, by making necessary approximations, an answer can be estimated, and software and computing capabilities of today have allowed these results to have actual real-life implications, which can be comfortably compared with experimental spectra. One of the earliest methods used for this purpose is the Hartree-Fock Molecular Orbital Theory. To understand, first consider the Schrodinger equation in its most basic form: $\hat{H}\Psi=E\Psi$

E is the total energy of the system, and $\hat{H}$ is described as the Hamiltonian, which specifies both the kinetic and potential energy for the particles.

$$\hat{H} = \left(-\frac{\hbar^2}{2m}\nabla^2 + \hat{V}\right)$$

To make a field as uniform as possible, each new point is taken as the average of the point before it:

(1) (2)

Figure 3.2: Uniform field being perturbed (1) and oscillating outwards (2)

If you perturb this uniform field, it will oscillate outwards, forming a wave. A wavefunction, Ψ, is the answer to the Schrodinger equation, which we approximate. Ψ must be single-valued, continuous and differentiable, normalizable, and orthogonal[12].

$$\int \left|\Psi^2\right| d\tau = 1 \qquad \int \Psi_n * \Psi_m d\tau = 0$$

Normalizable equation — Orthogonal equation

These equations can be modified to fit electronic calculations using the Born-Oppenheimer approximation, which assumes that from the perspective of orbiting electrons, the nucleus is stationary.

$$\hat{H}^{el}\Psi^{el} = E^{el}\Psi^{el}$$

The above equation removes the nuclear-nuclear Coulombic energy term. The next approximation that must be made takes into account the independence with which each of the electrons operate. The electrons move in complete independence from each other, and the Hartree-Fock approximation is used for this. Each of the electrons, N, in a system feel the average field of energy that all the other electrons feel, N-1, and the individual electrons are confined to spin orbitals. Because Ψ must be anti-symmetric, the Slater determinant must be zero in order for the wavefunction to be anti-symmetric, and it represents the electrons in different areas of the field moving, or interchanging. The setback for Hartree-Fock method is the assumption that electrons are paired, and as we will see, in many cases this is not always the case. Self-consistent field (SCF) theory is the procedure by which the lowest energy structure is obtained in computational chemistry using the Hartree-Fock method. From the above data, a set of equations called

the Hartree Fock equations are formed, each involving a single electron. Another approximation is then made called the linear combination of atomic orbitals approximation (LCAO) which allows the Hartree-Fock equations to be converted into algebraic equations, thus making them more solvable[7].

As computational chemistry has evolved, it has been discovered that the Hartree-Fock method is quite limiting in what can be discovered in the world of quantum chemistry software, so a number of new methods and approximations have been developed to compensate for this fact. It is important to remember that the more approximations are made for a theory to work, the farther it will be from the actual experimental results. The other theories are differentiated by their extent to which electron correlation is taken into account.

Density Functional Theory

In an effort to move past Hartree-Fock methods, density functional theory was created. The density functional theory is based on the availability of an exact solution for multi-electron systems and operates specifically under the idea of an electron gas with a uniform density[6]. An SCF formalism is used and the part of the solution that pertains only to the exchange and correlation contributions is extracted and placed inside the SCF formalism. The advantages of density functional theory surpass that of the Hartree-Fock method because it does not limit to an exact solution for the Schrodinger equation, but instead incorporates outside information (which is the solution created for the idealized problem)[7]. In DFT, the energy of the system is calculated as the sum of six components:

$$E_{DFT} = E_{NN} + E_T + E_V + E_{coul} + E_{exch} + E_{corr}$$

Where E_{NN} corresponds to the nuclear nuclear-repulsion, E_V corresponds to the nuclear-electron attraction, E_{coul} corresponds to the electron-electron Coulomb repulsion energies, E_T corresponds to the kinetic energy of the electrons, E_{exhc} corresponds to the non-classical electron-electron exchange energies, and E_{corr} corresponds to the correlated movement of electrons with different spins. Basically Density Functional Theory compensates for the more natural characteristics of the electrons in a system, including spin and interactions between electrons.

Optimizations and Frequencies

For the purposes of this experiment, each of the structures being studied was run in the Gaussian program to calculate the optimized lowest-energy structure, and further analyzed for the theoretical frequencies of the vibrations produced during Raman spectroscopy. Finding the optimized geometry of a structure is correlated to finding the lowest energy point on the potential energy surface (the bottom of the well). The optimization calculation does not necessarily consistently provide the lowest-energy structure, but it does ensure that the optimized structure does correspond to a local minima- that is, the optimized structure is definitely lower in energy than the original structure. The process of geometry optimization occurs by taking the first derivatives with respect to each of the geometrical coordinates, calculating the energy and energy gradient for the initial structure. These values are then used to take the first "step" towards optimizing the geometry, making a guess and then redirecting according to the energy of that guessed structure. In order for the guess to be correct, the energy gradient must approach zero[7].

A freq=raman command is used in the second round of calculations for each structure. This calculates the Raman frequencies that would theoretically appear in an experiment. Remember that in order for a vibration to be Raman active, there must be a change in the polarizability of the molecule during the vibration.

3B: Method and Basis Set

UB3LYP

B3LYP is a common method of the density functional theory, specifically a hybrid functional. The hybrid functional idea mixes exchange energies that are calculated in an exact manner with those from the density functional theory methods in order to ensure a better calculation.

The Becke-3-LYP (B3LYP) mixing scheme, using three mixing parameters[6]:

$E_{XC} = 0.2*E_X(HF) + 0.8*Ex(LSDA) + 0.72*DE_X(B88) + 0.1*E_C(LYP) + 0.19*E_C(VWN)$

The three scaling factors are derived by fitting the parameters to a set of thermochemical data. In the case of this experiment, the U is added to the B3LYP method, standing for unrestricted. This is added to allow for the calculation to optimize a structure with an unpaired electron- the 1-Hydroxyethyl radical has a lone electron on the O-C-C center carbon.

6-31++G(*d,p*)

6-31++G(*d,p*) is an example of a split-valence basis set. This is a minimal basis set corresponding to atoms with spherical coordinates and is composed of a stronger inner set and a looser outer set. However, the three Cartesian coordinates are treated separately, so they can correspond to a non-spherical atom. The split-valence basis set represents the core electrons by one set of functions and the outer electrons by another set of functions. The 6-31G basis sets have core orbitals represented with 6 Gaussians and valence orbitals are split into three and one Gaussian components[7]. The ++ added accounts for the hydrogen's diffuse s-type functions, which can be easily understood by considering how far away the electron is from the nucleus in a hydrogen atom (diffuse.) The d function and p functions are added to compensate for heavy atoms.[21]

aug-cc-pVTZ

cc-pVTZ is commonly known as a correlation consistent basis set, including the triple-zeta designation, which calculates three basis functions for each of the atomic orbitals present in the system. This allows the orbital itself to either grow or shrink when approached by other atoms in the system. It is important to note that a split-level basis set, as described before, calculates only one basis function for each of the atomic orbitals present in the molecule. By adding the "aug" prefix, this tells the program to add one set of diffuse functions for every angular momentum that is present in the basis.[21]

Chapter 4: Experimental Outline and Theoretical Results

4A: Experimental Setup

Matrix isolation Raman spectroscopy will be employed to experimentally study the interactions of 1-Hydroxyethyl radical and water. The matrix is required because the radical is unstable at room temperature and pressure, so the ideal conditions within the chamber will be roughly 10^{-8} Torr and 15 Kelvin. The reaction will take place on a gold plate within the chamber (5 in Figure 4.1). The experimental plan is to hit a solution of hydrogen peroxide and ethanol with radiation to produce the hydrogen peroxide radical. This radical will then be interacted with ethanol to produce 1-Hydroxyethyl radical and water. This reaction will take place on a gold plate inside the matrix chamber, and using cryotechnology, the final products will be frozen down, warmed up slightly to react, and then frozen down again so that the radical can be analyzed by Raman spectroscopy. A fiber optic cable will be used to collect the Raman scattering within the chamber (6 in Figure 4.1), and the Ocean Optics program is employed to analyze and quantify the data.

Matrix Isolation Raman Spectrometer

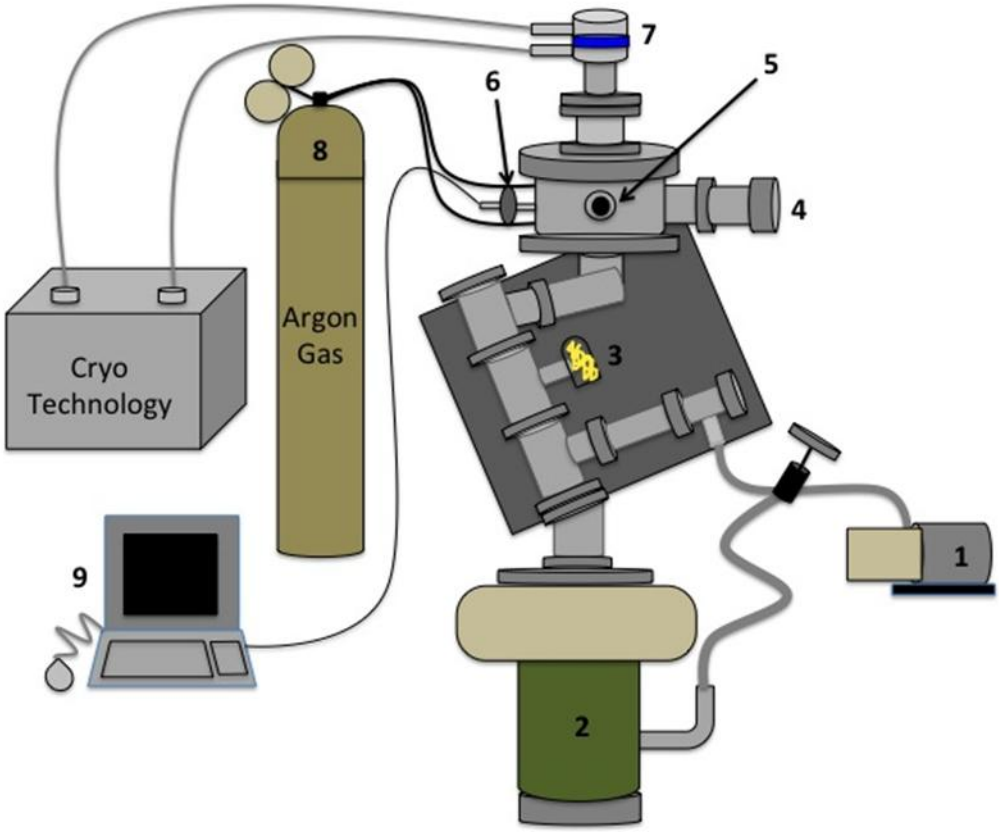

Figure 4.1: Schemata of a Matrix Isolation Raman

1: Roughing pump: works to pressurize the chamber to the minimum fore-pressure required to turn on the diffusion pump. Roughing pump generally gets the pressure to $10^{-2} - 10^{-3}$ Torr.

2: Diffusion pump: further pressurizes the chamber to between 10^{-6} and 10^{-8} Torr. Vacuum pressure is required to study radicals because they are unstable at room temperature and pressure. Manipulation of the conditions allows for prolonged measurement of the interactions of the radical with surrounding water molecules. A

diffusion pump works by a series of spinning metal cones and silicon-based diffusion pump oil.

3: Ionization gauge: measures the pressure at extremely low values. Ionization gauges work by ionizing particles inside the vacuum on a heated coil, which converts the readings to a digital readout in Torr.

4: Window #1: large window at one end of the matrix chamber. This allows for proper positioning of the lens and fiber optic on the matrix inside the chamber for maximum Raman scattering data output.

5: Window #2: small window in the wall of the matrix chamber. This window allows the laser light to pass into the chamber and hit the matrix, thus causing scattering of radiation and allowing Raman analysis.

6: Fiber optic cable: a small, portable cable that converts the raw Raman scattering data into the spectra we see in the Ocean Optics program. This takes binary data and converts it into a digital domain with the axes intensity (power) versus wavenumbers.

7: Cryotechnology: the inlet through which the temperature can be controlled in the matrix chamber. Ideal temperature is around 15 Kelvin, thus allowing the radical to be frozen onto the gold-plated matrix. Throughout the experiment, the temperature will be altered in small increments so as to allow the radical and water molecules to interact, before freezing them back into place onto the matrix for spectral analysis.

8: Gas inlet: the connection from a gas tank, most commonly argon, to the matrix chamber. In order to freeze the radical and water onto the gold plate, there must be a gas solvent. An argon matrix is the most common for this purpose.

9: The computer used in this type of spectral analysis employs a program called Ocean Optics.

4B: Results: Lowest-Energy Structures

Optimized radical structure:

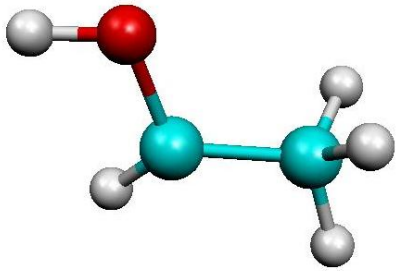

Figure 4.2: 1HEOfreq.out

Optimized radical with one water structures:

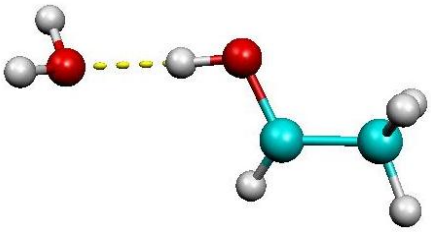

Figure 4.2.1: B

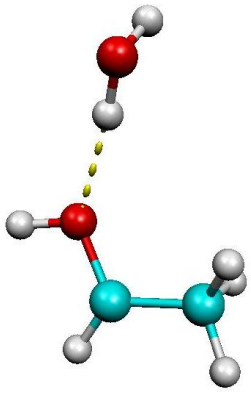

Figure 4.2.2: A

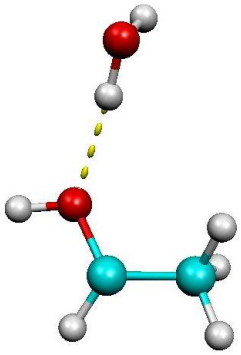

Figure 4.2.3: E

Optimized radical with two waters structures:

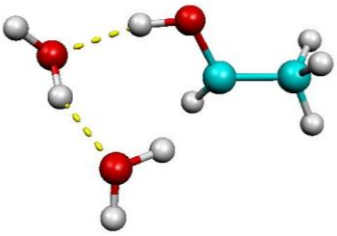

Figure 4.2.4: B2

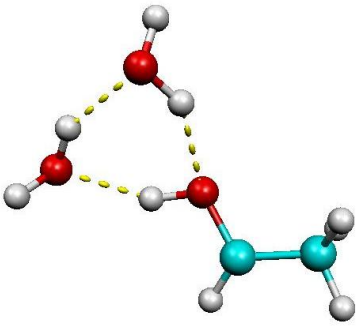

Figure 4.2.6: A2

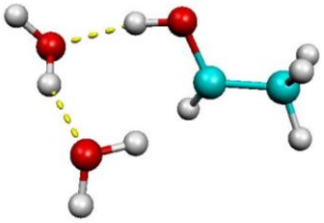

Figure 4.2.5: B3

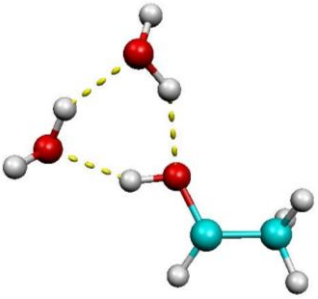

Figure 4.2.7: A3

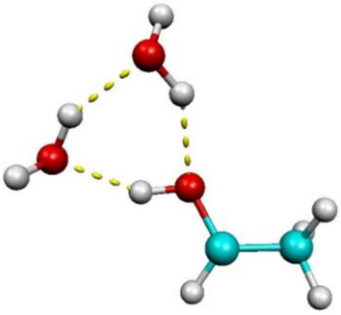

Figure 4.2.9: E2

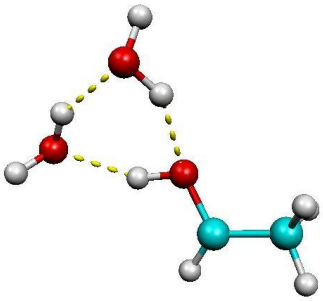

Figure 4.2.8: B

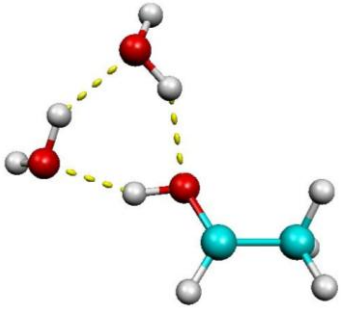

Figure 4.3: E

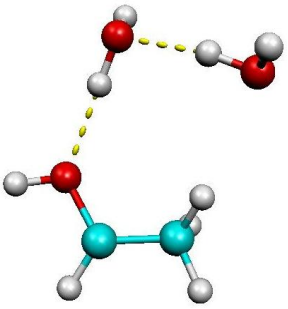

Figure 4.3.2: E3

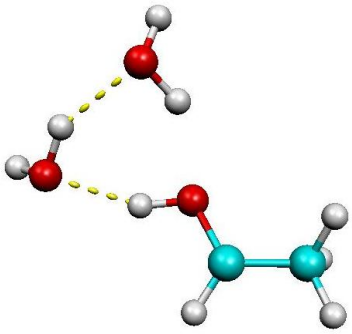

Figure 4.3.1: A

Optimized radical with three waters structures:

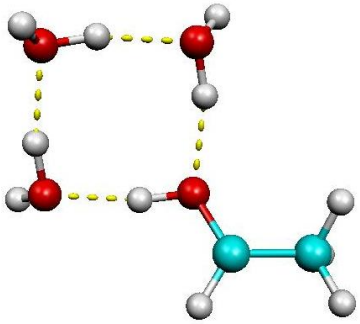

Figure 4.3.3: E2

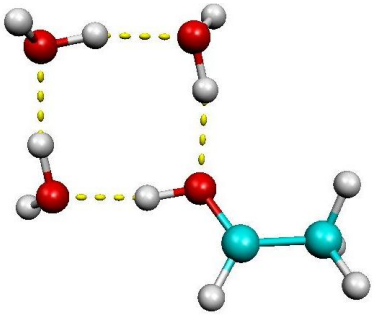

Figure 4.3.4: E3

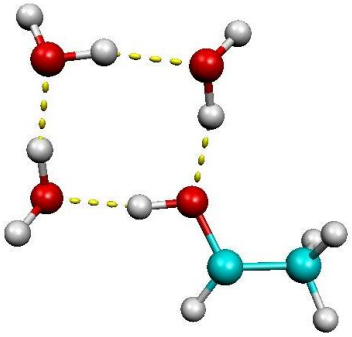

Figure 4.3.5: D2

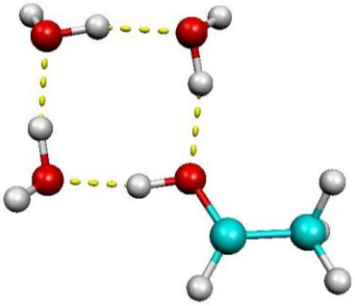

Figure 4.3.6: D3

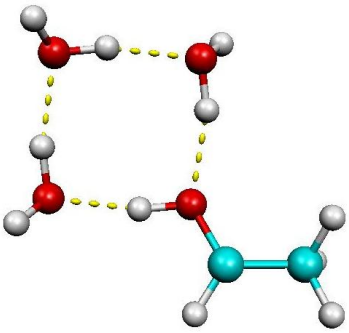

Figure 4.3.7: A

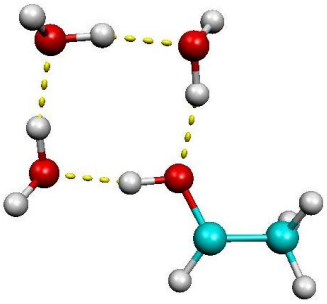

Figure 4.3.8: A2

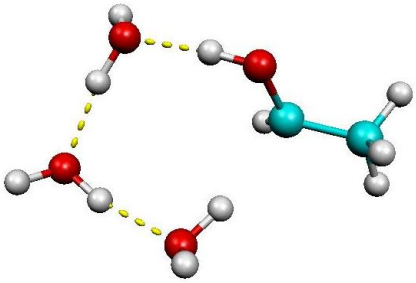

Figure 4.3.9: C3

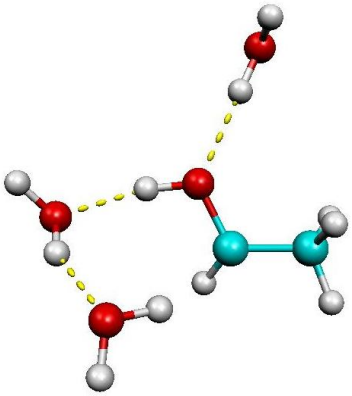

Figure 4.4: C

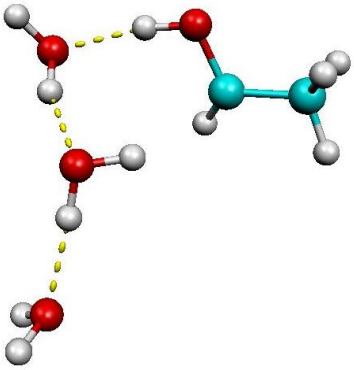

Figure 4.4.1: B2.out

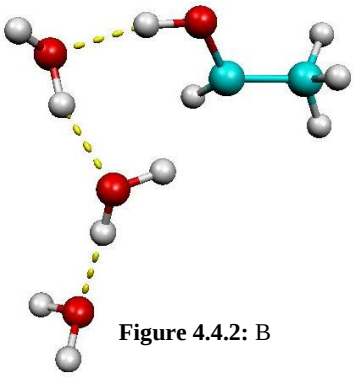

Figure 4.4.2: B

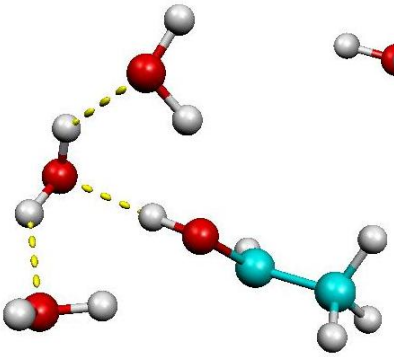

Figure 4.4.3: D

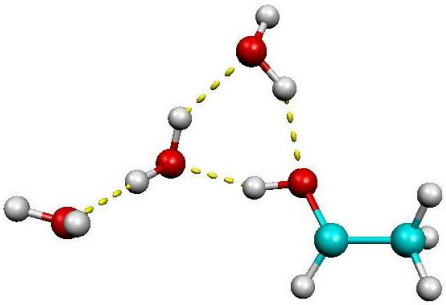

Figure 4.4.4: A3

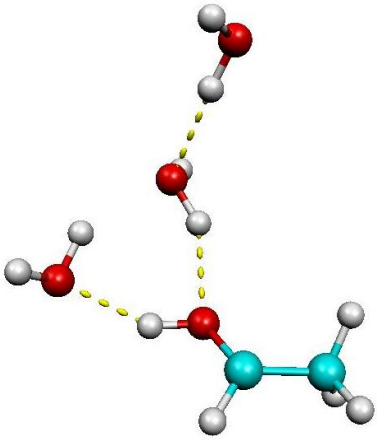

Figure 4.4.5: B3

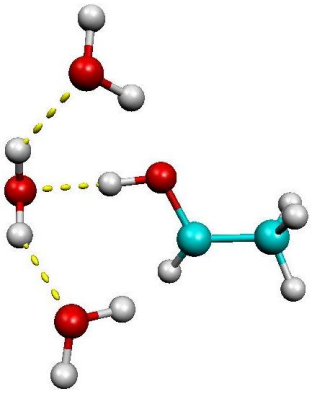

Figure 4.4.6: C2

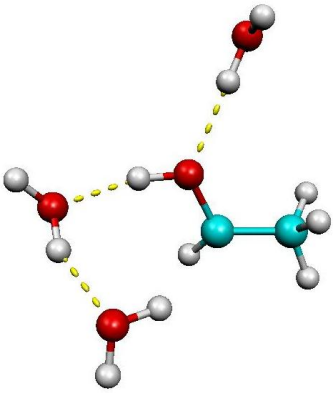

Figure 4.4.7: E

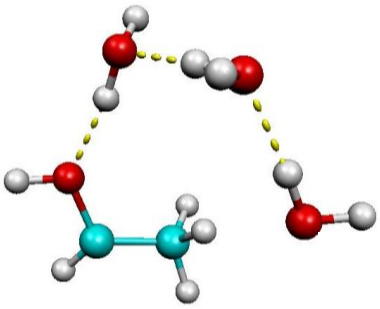

Figure 4.4.8: F2

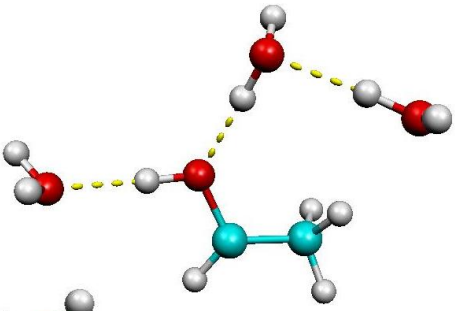

Figure 4.5: F3

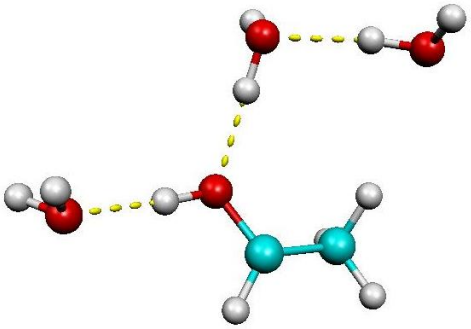

Figure 4.4.9: F

Optimized radical with four waters structures:

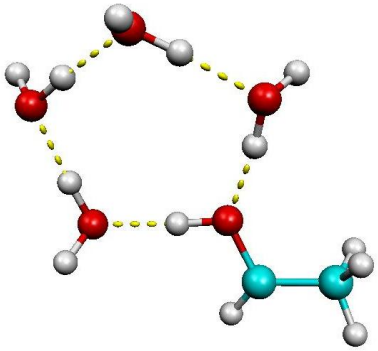

Figure 4.5.1: G2

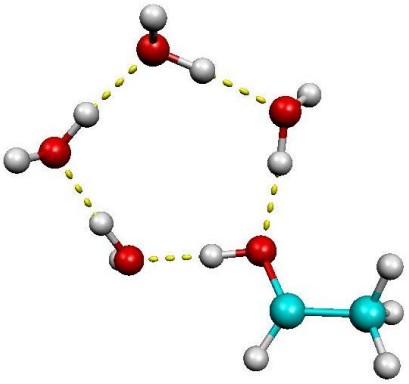

Figure 4.5.3: A3

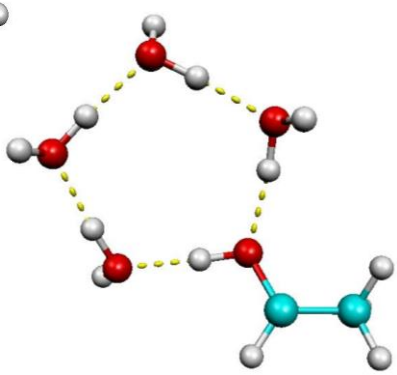

Figure 4.5.2: H3

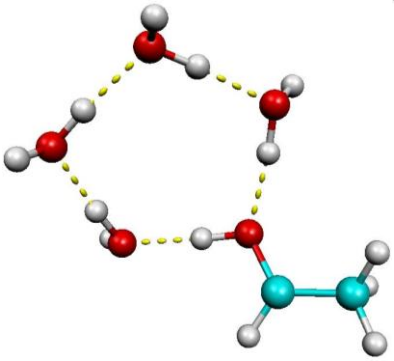

Figure 4.5.4: K3

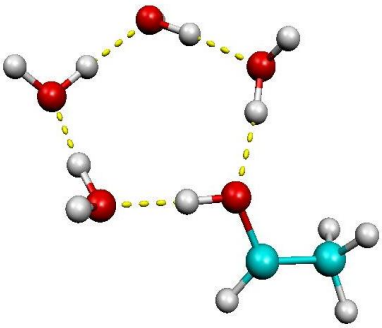

Figure 4.5.6: C2

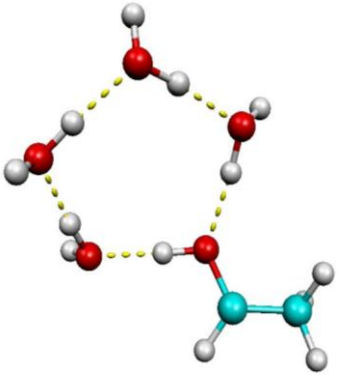

Figure 4.5.5: F

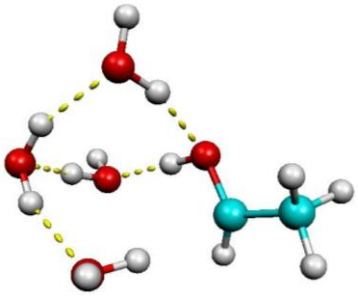

Figure 4.5.7: K

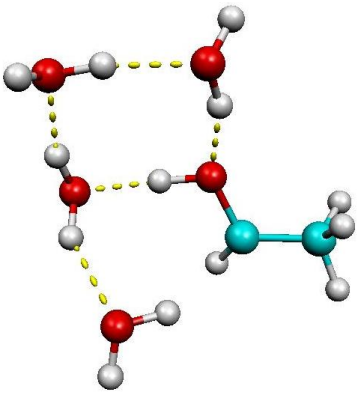

Figure 4.5.9: D

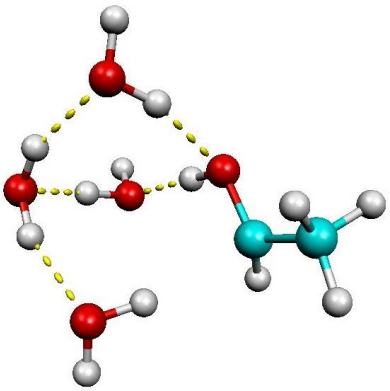

Figure 4.5.8: E3

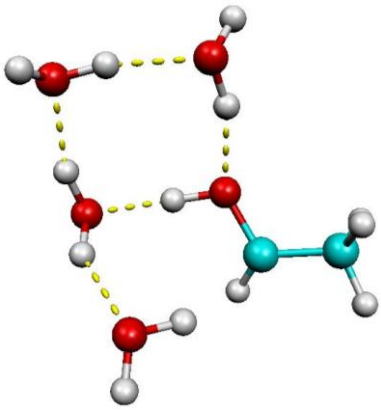

Figure 4.6: B2

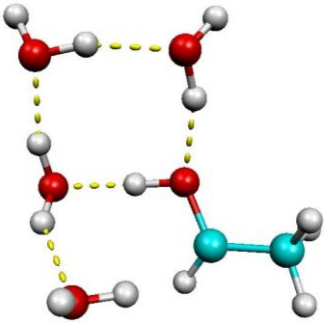

Figure 4.6.2: I3

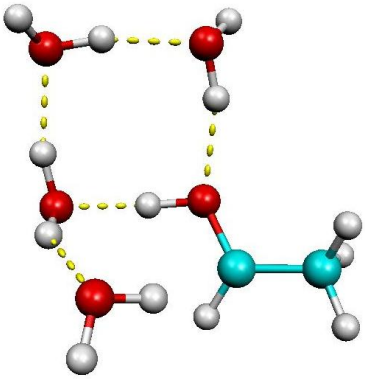

Figure 4.6.1: B3

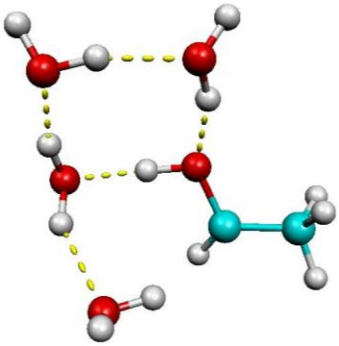

Figure 4.6.3: I

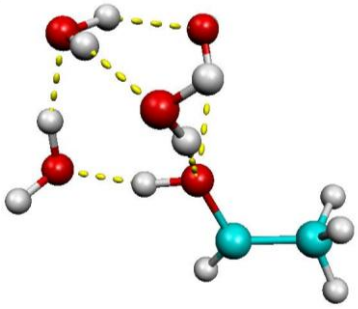

Figure 4.6.5: H

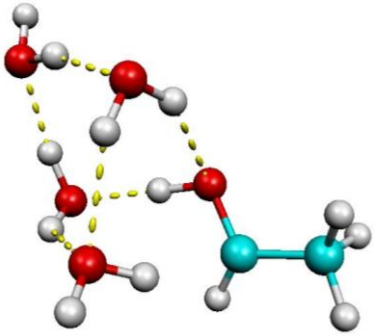

Figure 4.6.4: F3

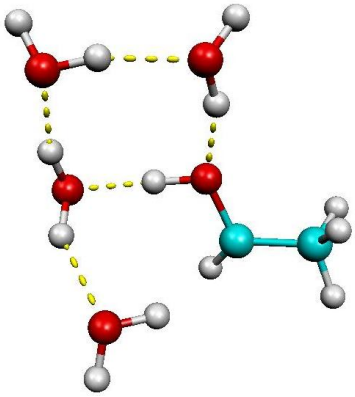

Figure 4.6.6: E2

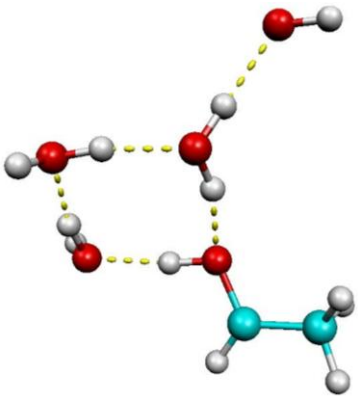

Figure 4.6.8: K2

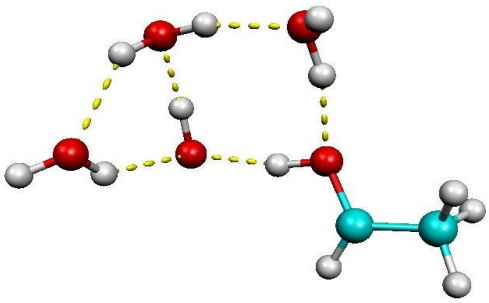

Figure 4.6.7: C3

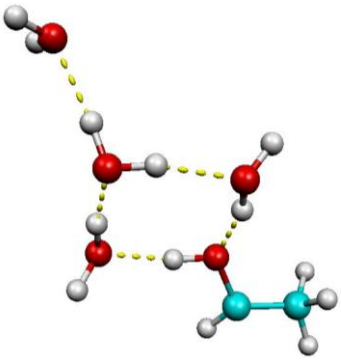

Figure 4.6.9: I2

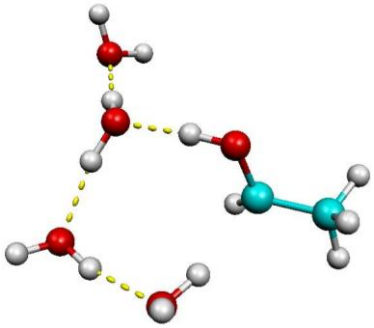

Figure 4.7.1: A

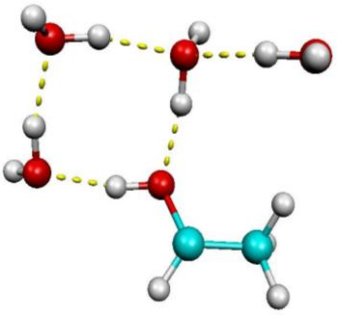

Figure 4.7: L3

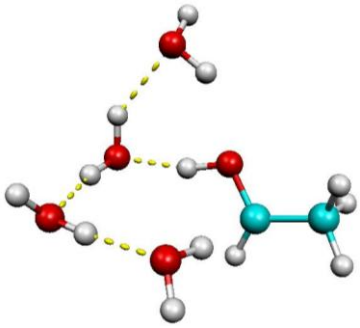

Figure 4.7.3: H2

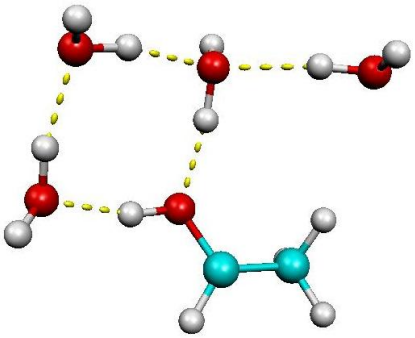

Figure 4.7.5: A2

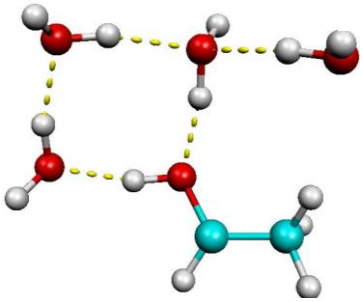

Figure 4.7.4: L2

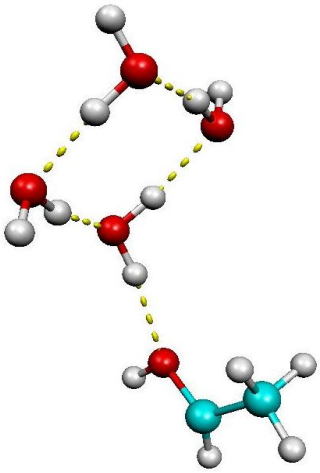

Figure 4.7.6: J2

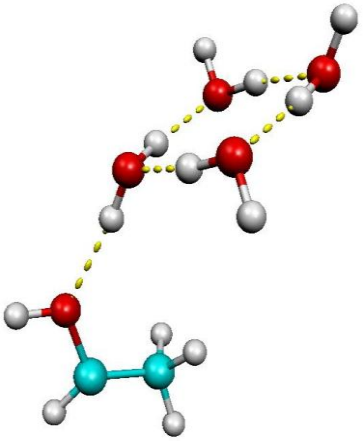

Figure 4.7.8: J

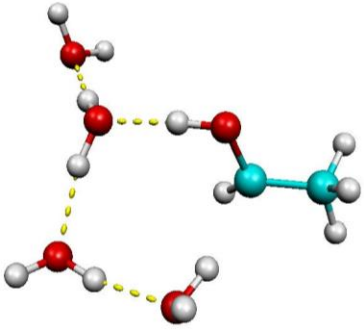

Figure 4.7.9: G

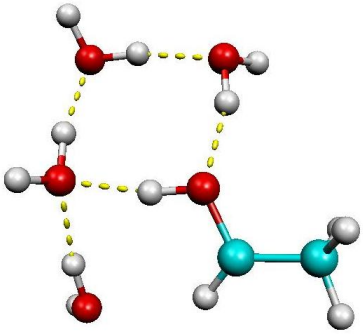

Figure 4.8: G3

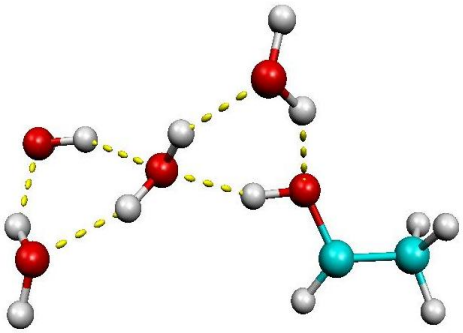

Figure 4.8.2: B

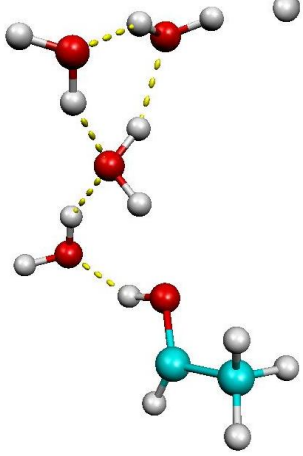

Figure 4.8.1: L

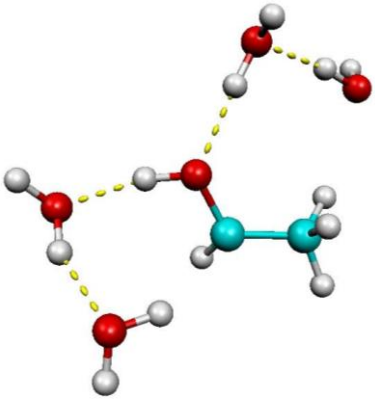

Figure 4.8.3: D2

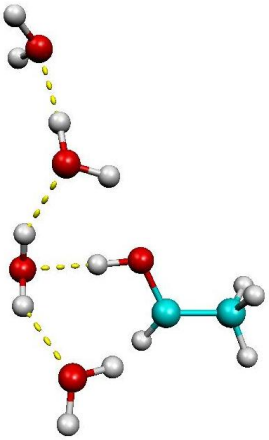

Figure 4.8.5: E

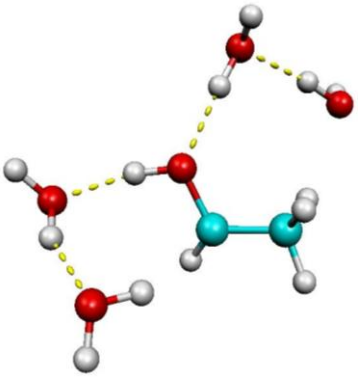

Figure 4.8.4: D3

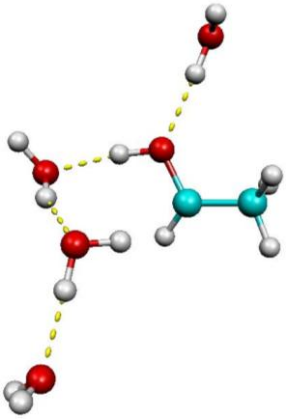

Figure 4.8.6: F2

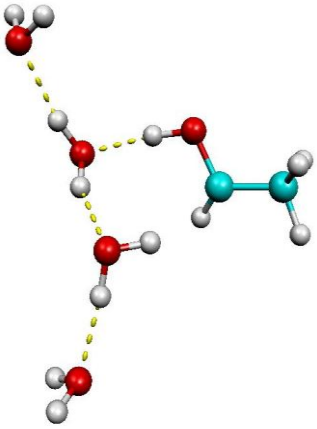

Figure 4.8.7: C

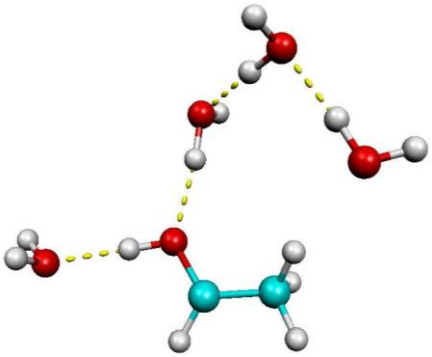

Figure 4.8.8: J3

Optimized radical with five waters structures:

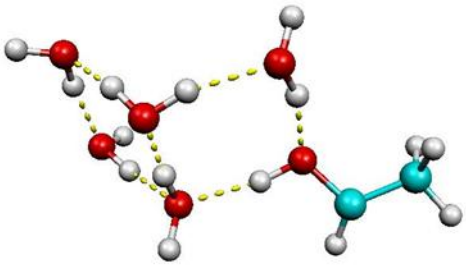

Figure 4.8.9: N2

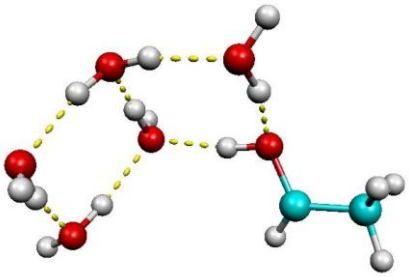

Figure 4.9.1: W

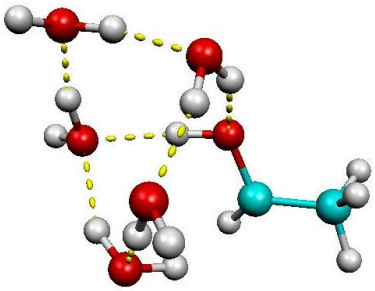

Figure 4.9: P

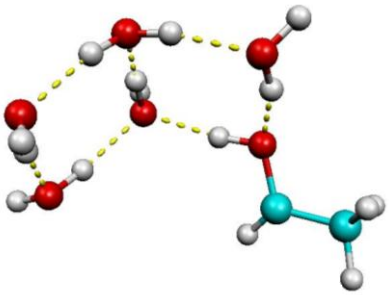

Figure 4.9.2: X2

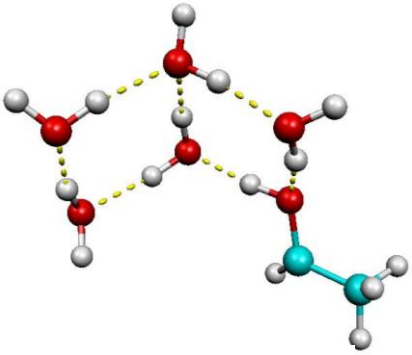

Figure 4.9.4: Q2

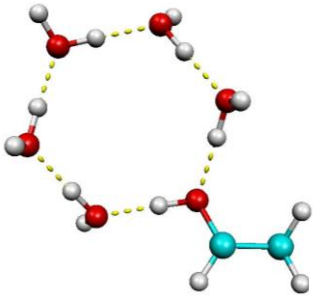

Figure 4.9.3: A2

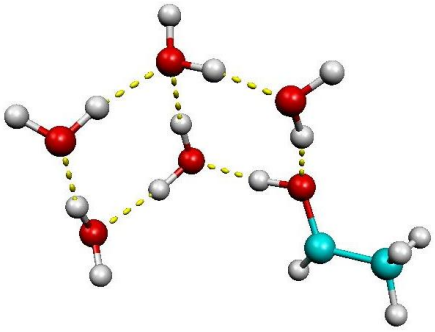

Figure 4.9.5: T2

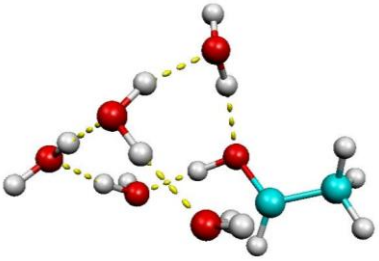

Figure 4.9.7: X

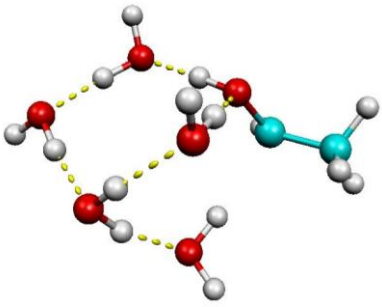

Figure 4.9.6: K3

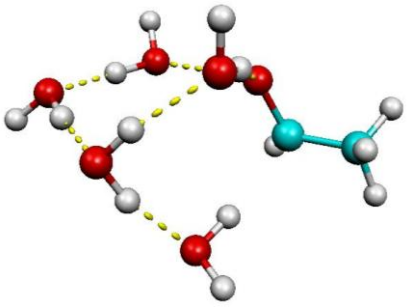

Figure 4.9.9: K2

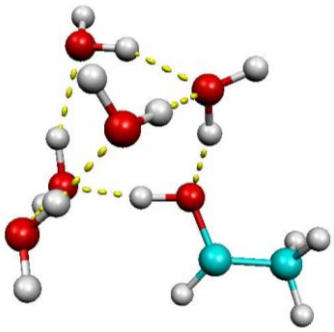

Figure 5.1: BB

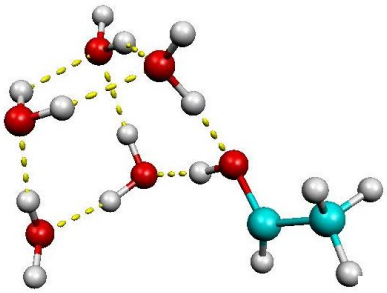

Figure 5.0: T3

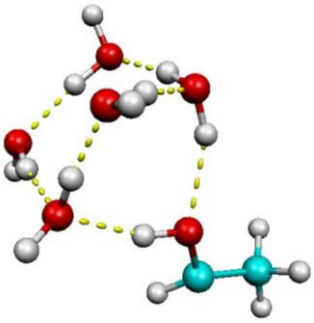

Figure 5.1.1: L2

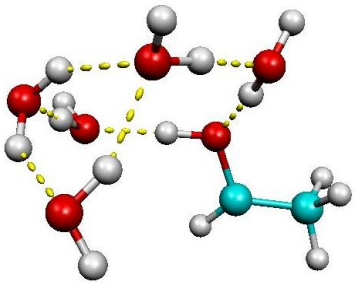

Figure 5.1.3: Z

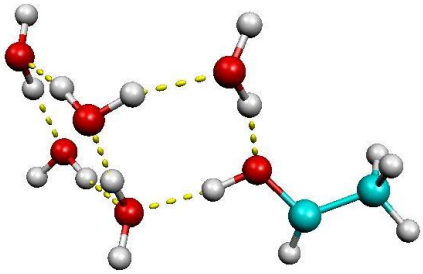

Figure 5.1.2: R2

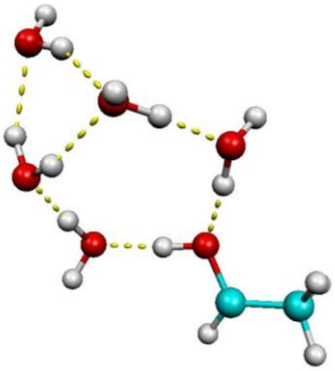

Figure 5.1.4: J

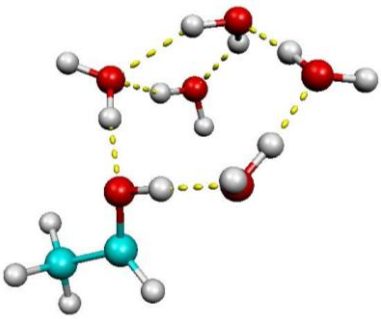

Figure 5.1.6: AA2

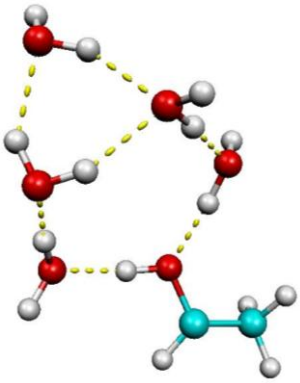

Figure 5.1.5: J3

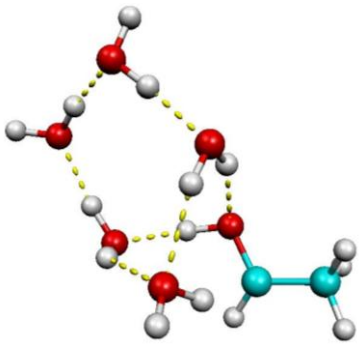

Figure 5.1.7: E2

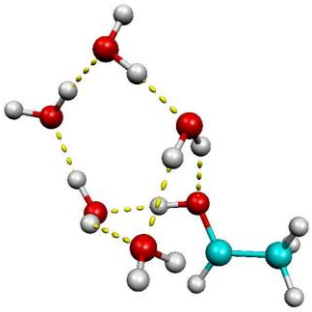

Figure 5.1.8: D3

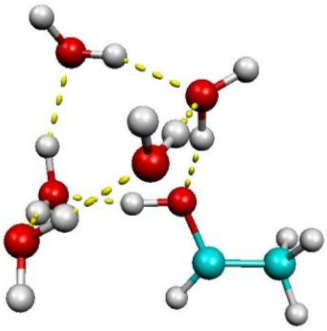

Figure 5.1.9: V

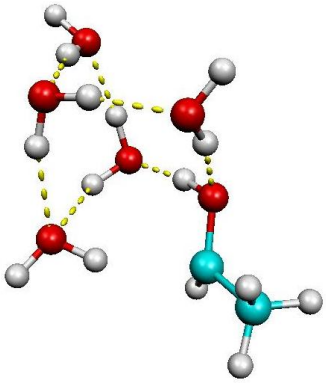

Figure 5.2: S

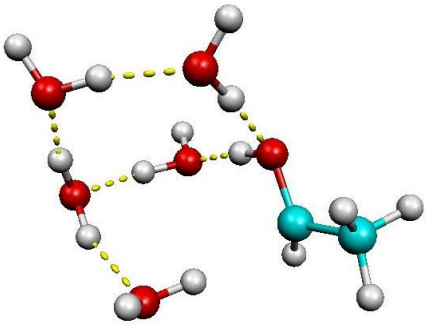

Figure 5.2.3: AA

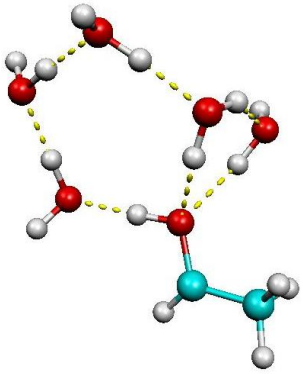

Figure 5.2.1: CC3

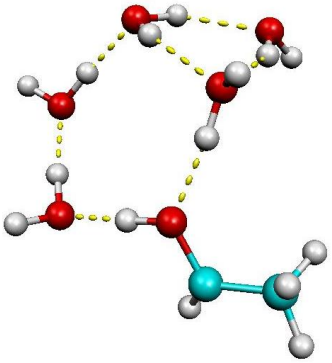

Figure 5.2.4: Y2

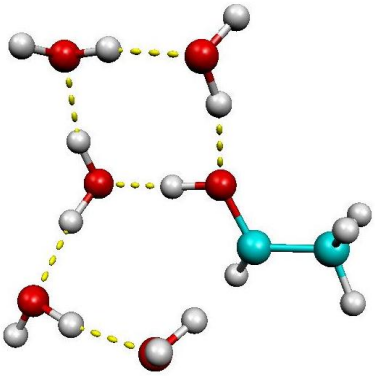

Figure 5.2.5: U3

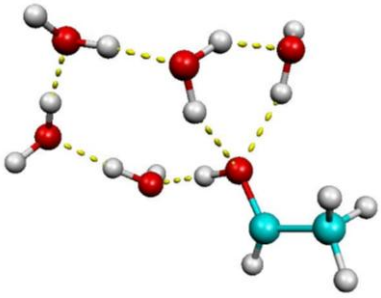

Figure 5.2.6: AA3

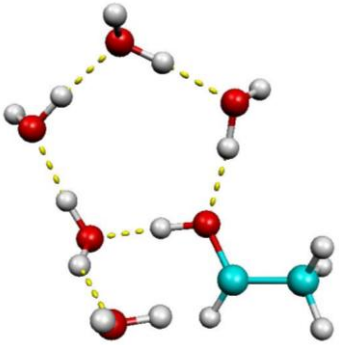

Figure 5.2.8: CC2

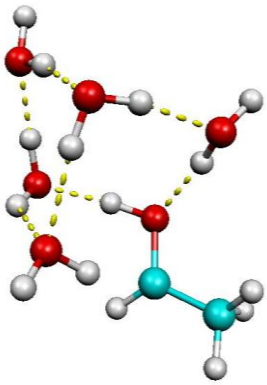

Figure 5.2.7: S2

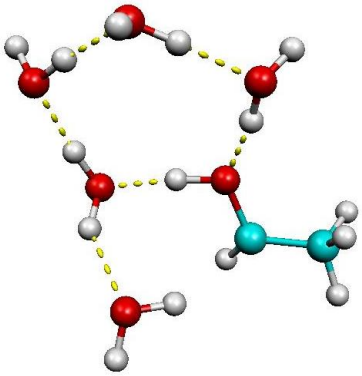

Figure 5.2.9: U2

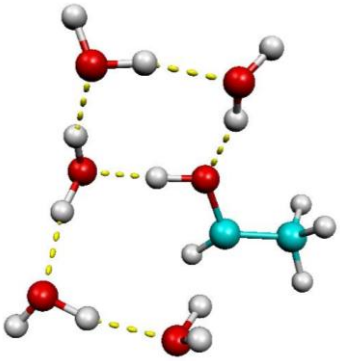

Figure 5.3.1: Q3

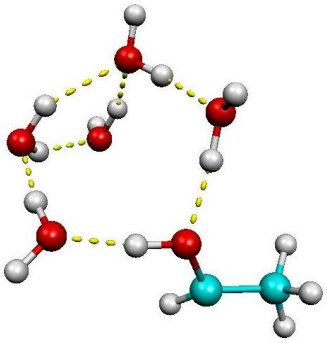

Figure 5.3: C

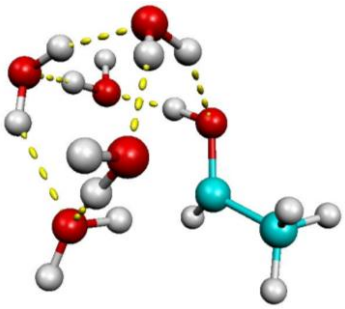

Figure 5.3.2: W3

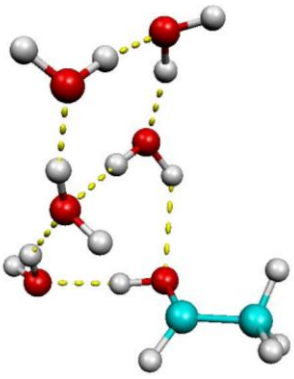

Figure 5.3.4: E3

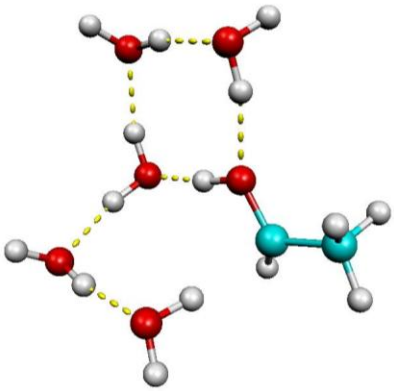

Figure 5.3.3: V3

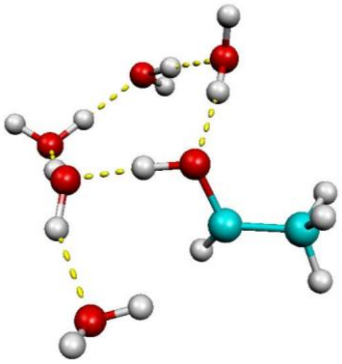

Figure 5.3.5: BB2

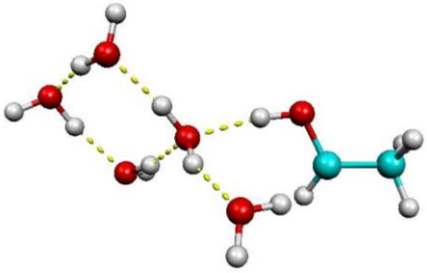

Figure 5.3.6: D

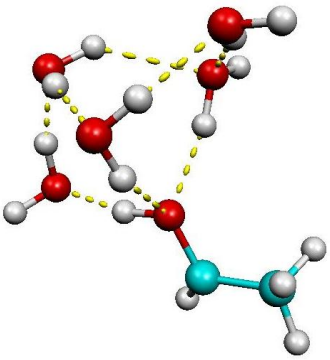

Figure 5.3.7: R

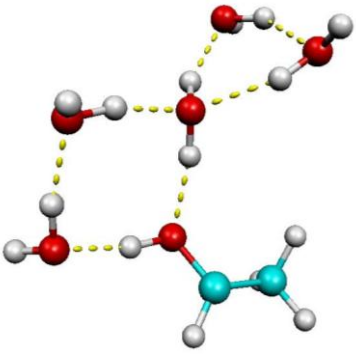

Figure 5.3.8: M

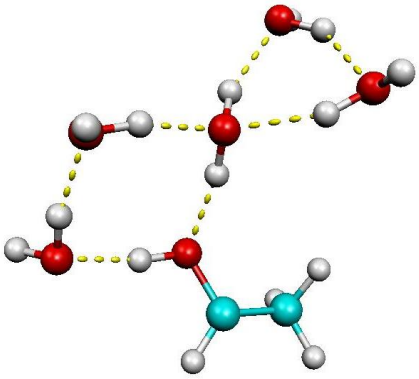

Figure 5.3.9: O

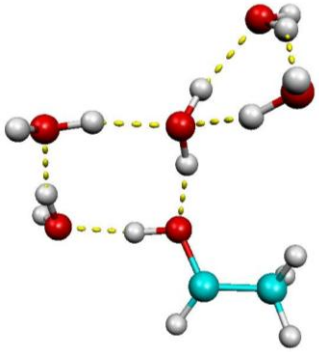

Figure 5.4: G3

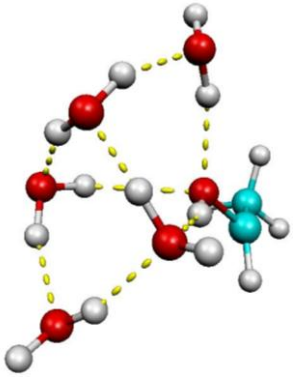

Figure 5.4.1: R3

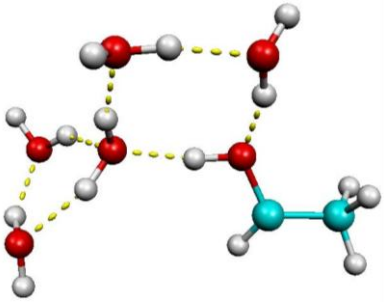

Figure 5.4.2: L

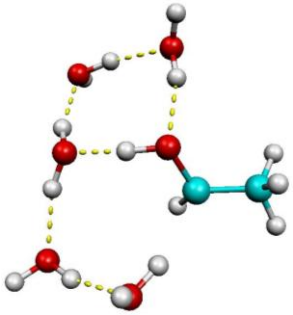

Figure 5.4.3: H2

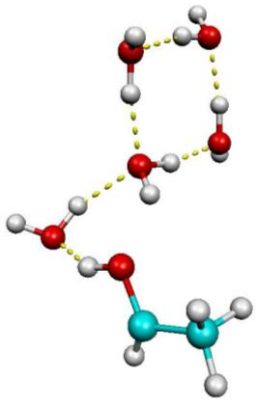

Figure 5.4.4: A3

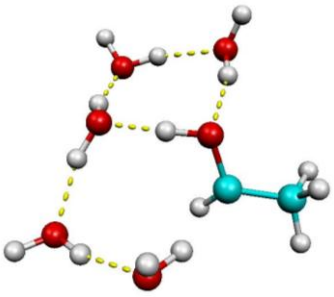

Figure 5.4.6: H3

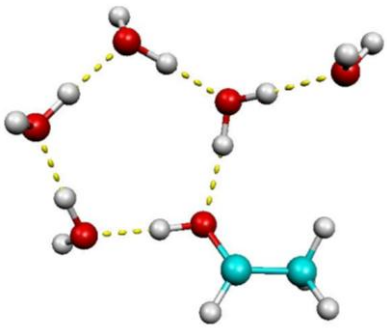

Figure 5.4.5: Z3

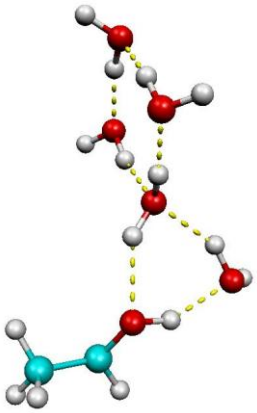

Figure 5.4.7: G

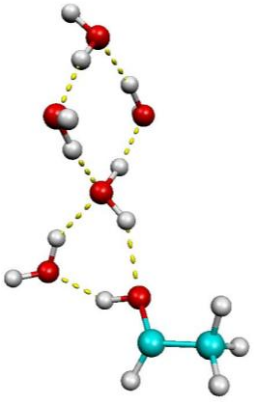

Figure 5.4.9: G2

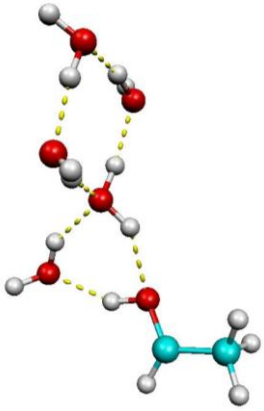

Figure 5.4.8: I

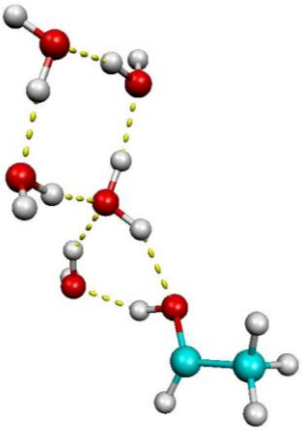

Figure 5.5.2: I3

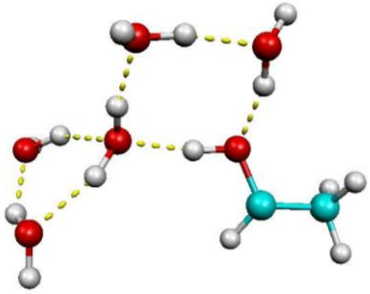

Figure 5.5: F3

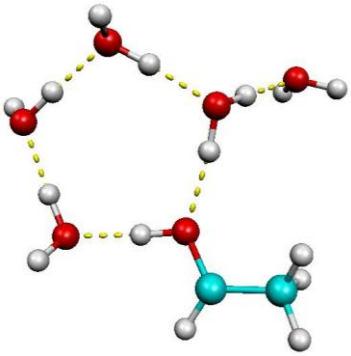

Figure 5.5.1: CC

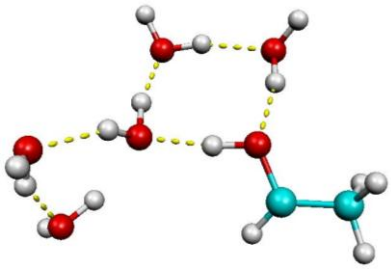

Figure 5.5.3: C3

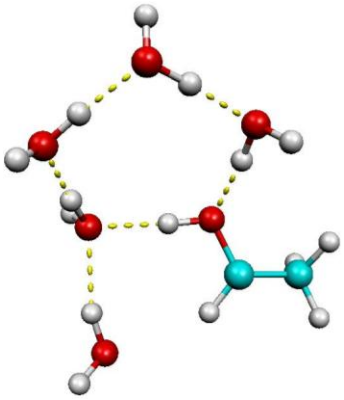

Figure 5.5.4: BB3

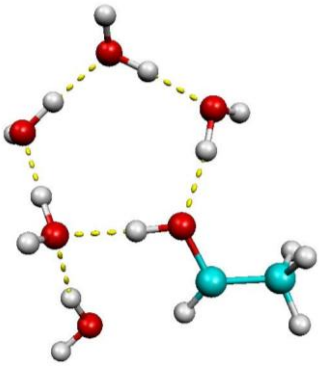

Figure 5.5.5: L3

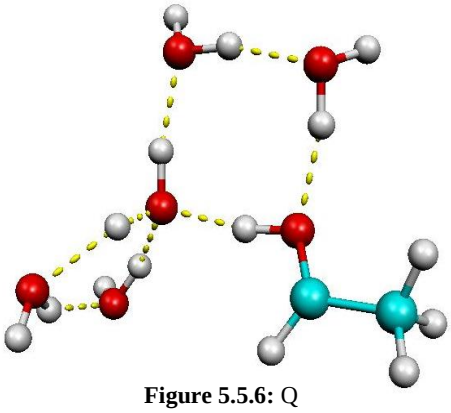

Figure 5.5.6: Q

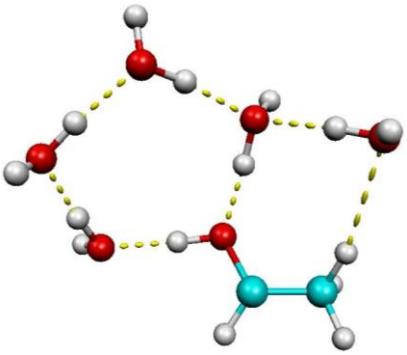

Figure 5.5.8: Z2

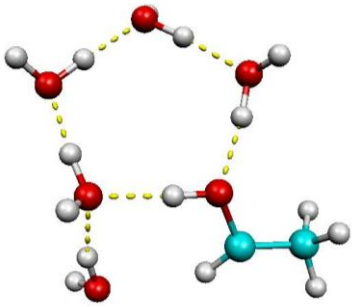

Figure 5.5.7: Y

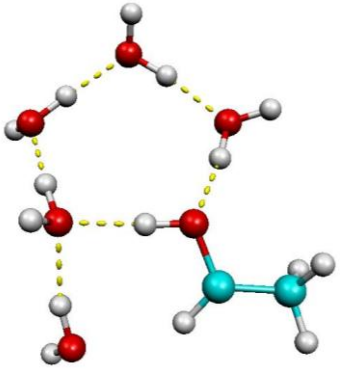

Figure 5.5.9: J2

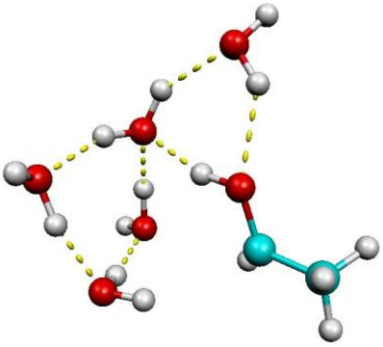

Figure 5.6.1: K

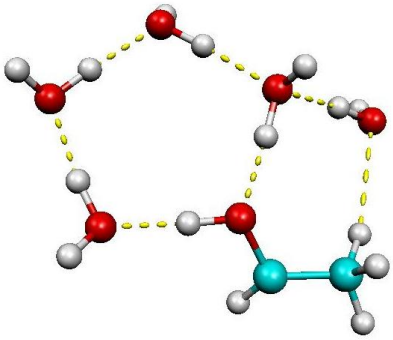

Figure 5.6: Y3

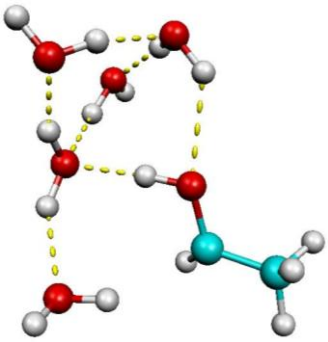

Figure 5.6.2: T

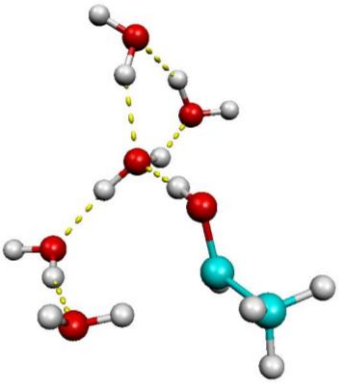

Figure 5.6.3: H

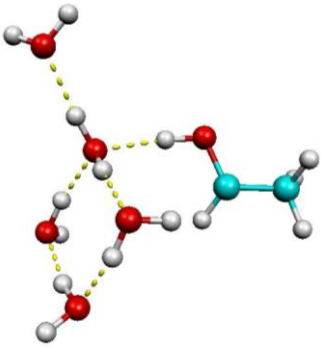

Figure 5.6.4: B3

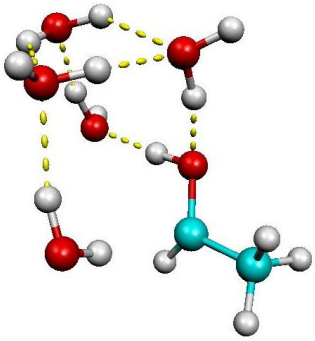

Figure 5.6.5: M2

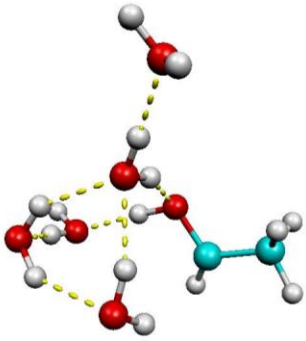

Figure 5.6.6: O2

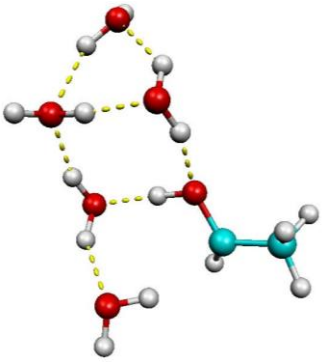

Figure 5.6.7: V2

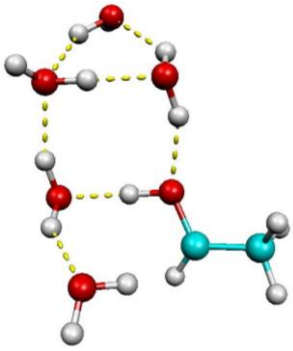

Figure 5.6.8: U

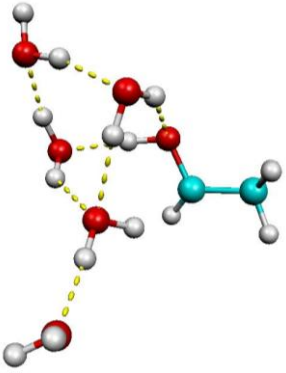

Figure 5.6.9: B2

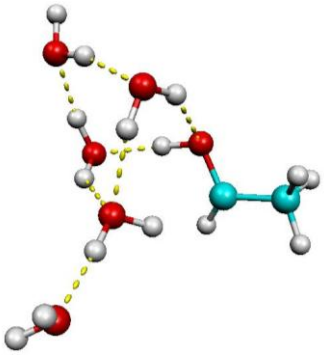

Figure 5.7: S3

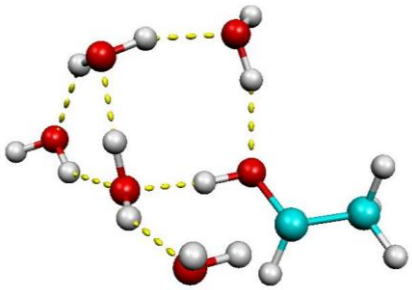

Figure 5.7.1: D2

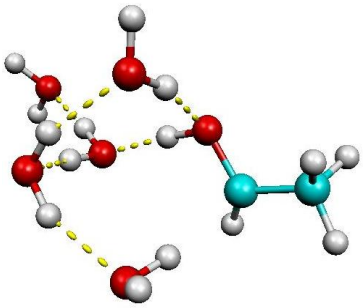

Figure 5.7.2: X3

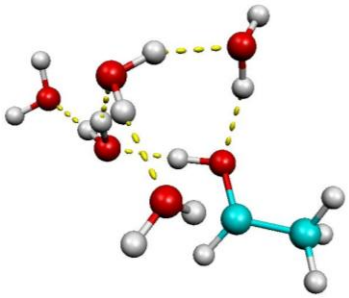

Figure 5.7.3: W2

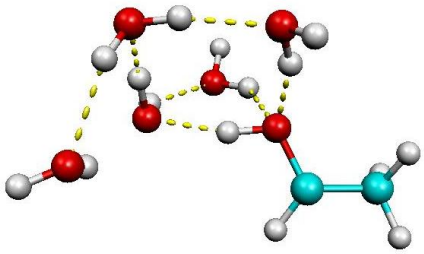

Figure 5.7.4: P2

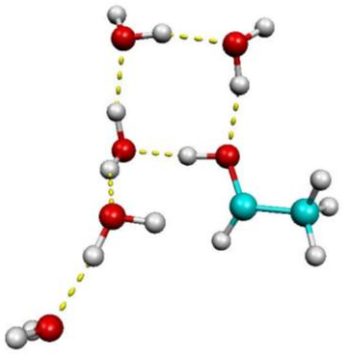

Figure 5.7.5: B

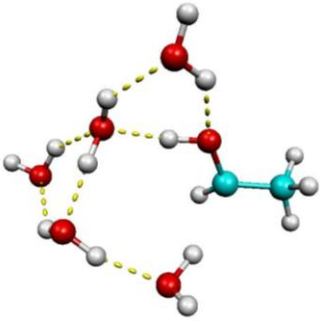

Figure 5.7.6: F2

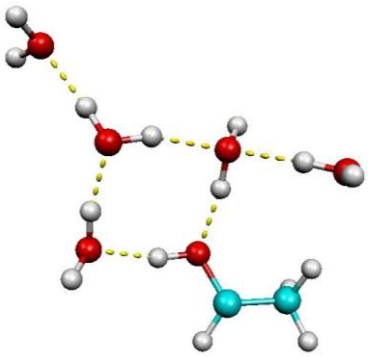

Figure 5.7.7: N

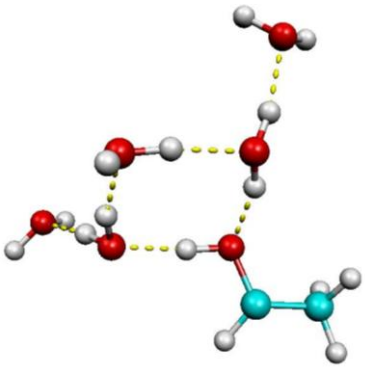

Figure 5.7.8: O3

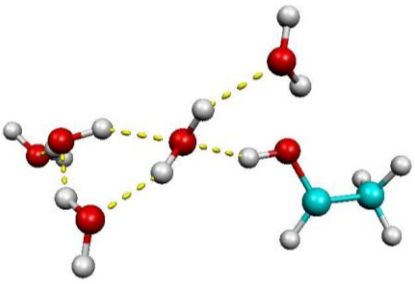

Figure 5.7.9: F

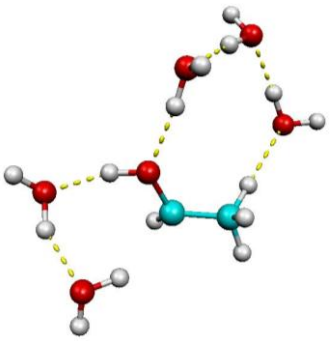

Figure 5.8: E

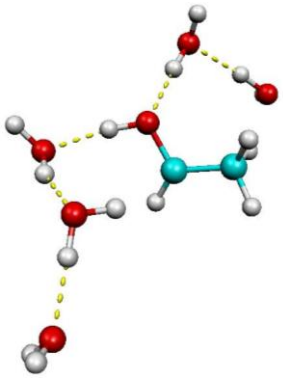

Figure 5.8.2: C2

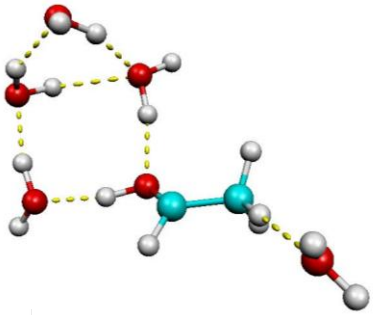

Figure 5.8.1: M3

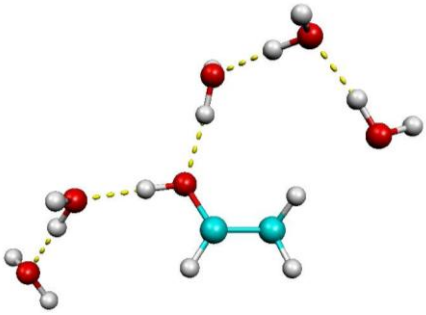

Figure 5.8.3: A

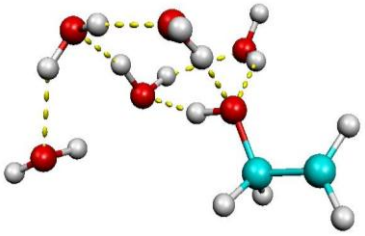

Figure 5.8.5: P3

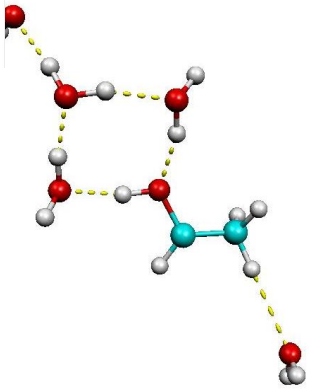

Figure 5.8.4: N3

It is important to note that the five water calculations are not finished being run on the aug-cc-pVTZ basis set, so the images in this thesis are of the optimized 6-31++G(*d*,*p*) basis set.

Structure	Energy, kcal/mol	Binding Energy, kcal/mol	Binding Energy per Water Molecule, kcal/mol
0w	-9.69×10^4	--	--
1w	-1.45×10^5	5.48	5.48
2w	-1.93×10^5	14.65	7.32
3w	-2.41×10^5	25.84	8.61
4w	-2.89×10^5	34.77	8.69
5w	-3.37×10^5	--	--

Table 4.1: Optimized lowest-energy structure energies (displayed in kcal/mol) and calculated binding energies of the water molecules for each structure. These values were calculated using the UB3LYP method and aug-cc-pVTZ basis set (except for the 5w; these are still currently being run on aug-cc-pVTZ, and are shown after being calculated with the 6-31++G(*d,p*) basis set).

The energy of a single water molecule (optimized structure in Gaussian) is equal to -76.4661965 Hartrees. Using this value, the binding energies of each water molecule was found by subtracting the energy of the radical from the overall energy of the structure. Following this, the optimized energy of a single water molecule previously calculated in Gaussian using the same aug-cc-pVTZ basis set was subtracted from the [Overall Energy – Radical Energy] value to arrive at the binding energy for the total water molecules in the optimized structures. To determine the single binding energy of each water molecule, the total binding energy was divided by the number of water molecules added. The 5w binding energies are left blank because they are currently being run on the aug-cc-pVTZ basis set, but are not quite finished yet. The energies produced cannot be compared because they are of the 6-31++G(*d,p*) basis set.

Lowest-Energy Structures and Theoretical Raman Spectra

The lowest-energy structures of 1-Hydroxyethyl radical in various cluster sizes were optimized using the augmented triple-zeta basis set, aug-cc-pVTZ and the Raman vibrational frequencies were calculated. The Raman spectra were then simulated using a LabView program created by the Hammer Lab called SpectrumSimulator which plots the data points from the freq=raman output file under Raman spectroscopic parameters. There are several unique peaks in the spectrum that correspond to specific vibrational motions that remain consistent, although shifted, in all of the lowest-energy structures for the radical in increasing solvation matrices. Below are the simulated Raman spectra for the lowest-energy structures of each increasing cluster size.

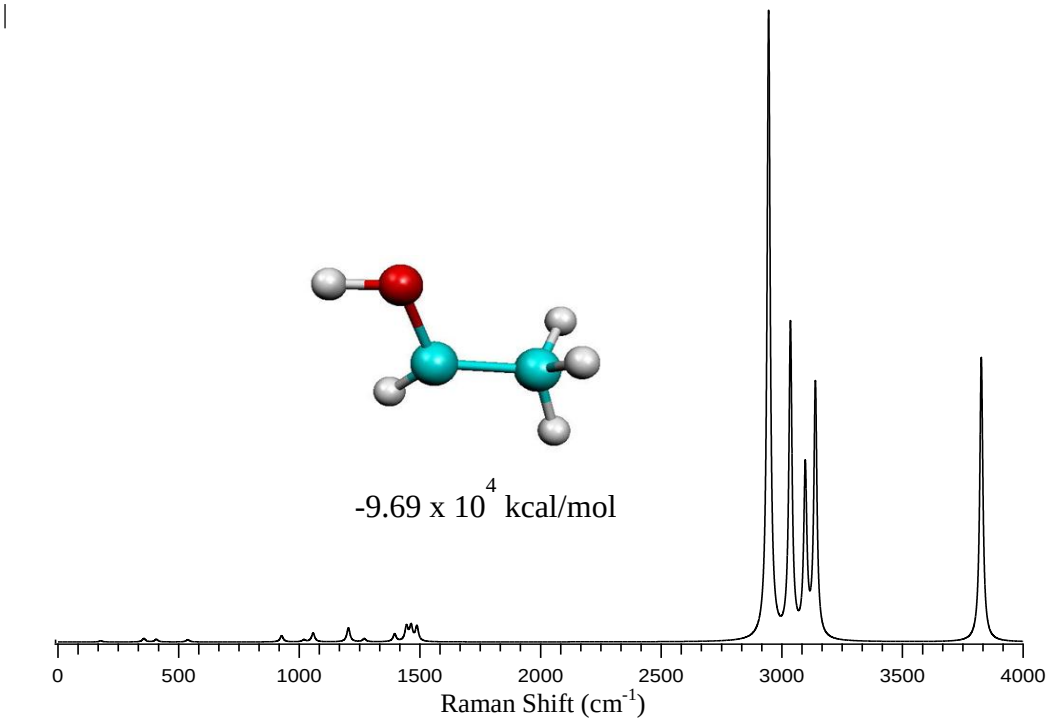

Figure 5.8.7: Simulated Raman spectra for the optimized lowest-energy structure of 1-Hydroxyethyl radical.

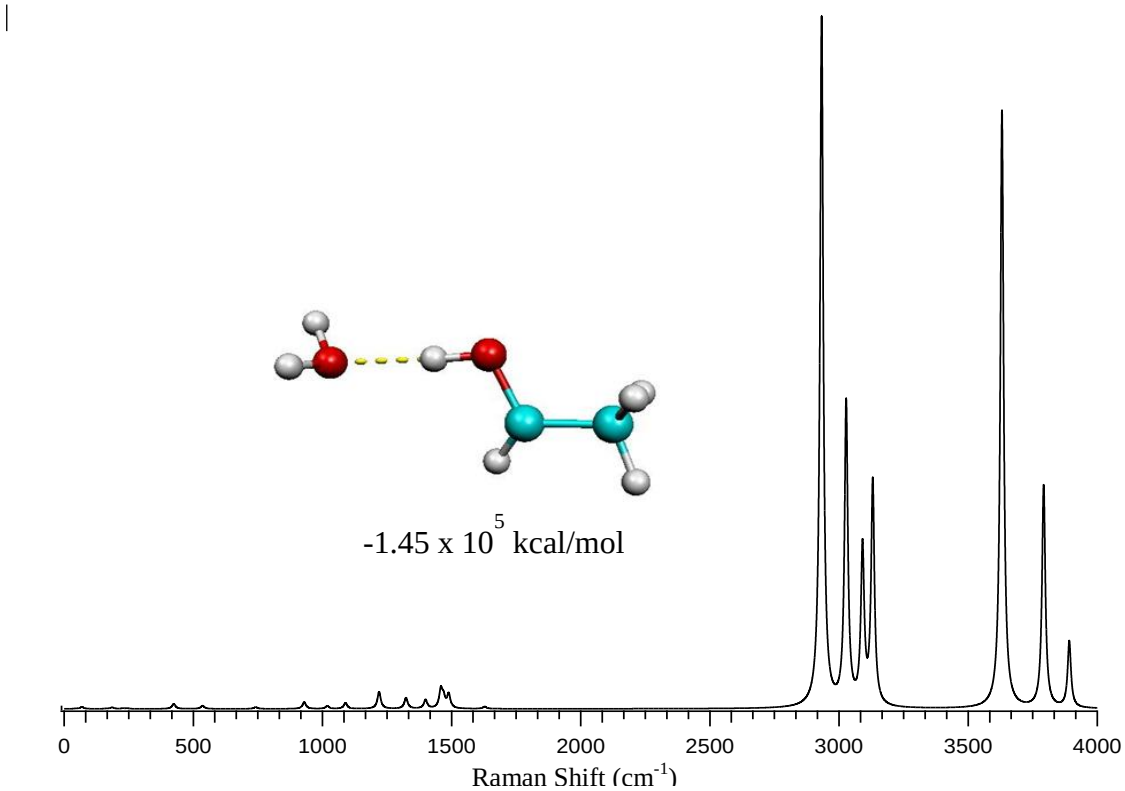

Figure 5.8.8: Simulated Raman spectra for the optimized lowest-energy structure of 1-Hydroxyethyl radical with one water molecule.

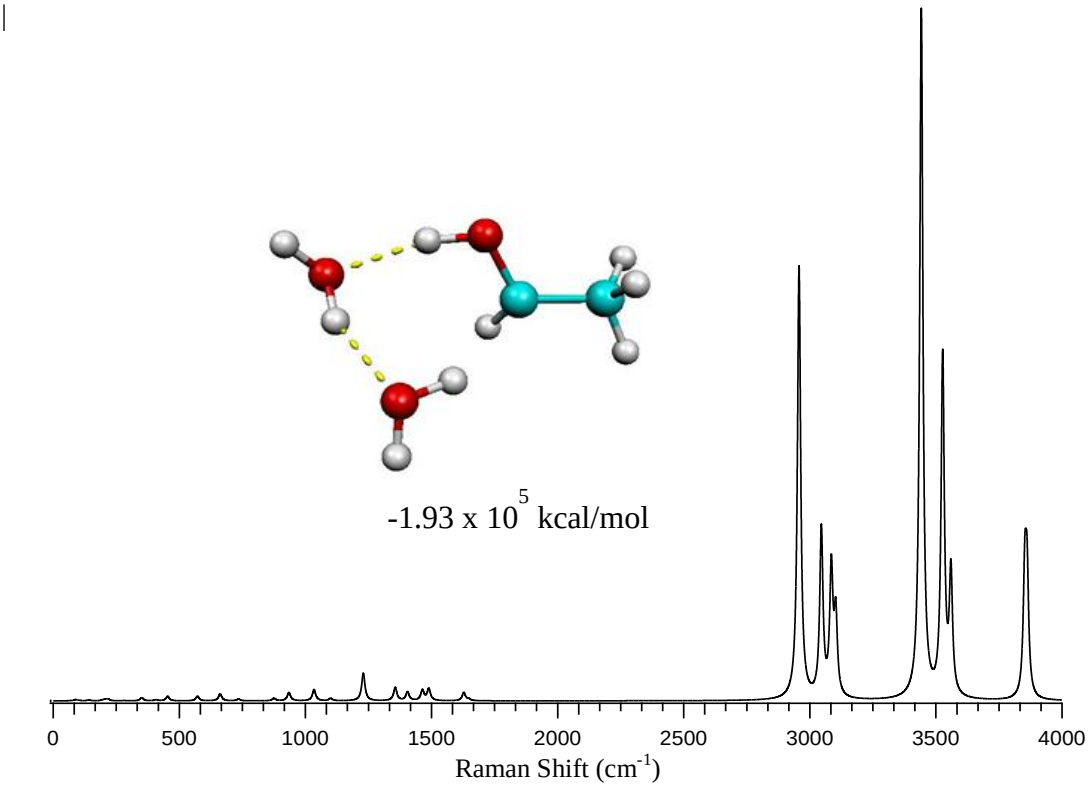

Figure 5.8.9: Simulated Raman spectra for the optimized lowest-energy structure of 1-Hydroxyethyl radical with two water molecules.

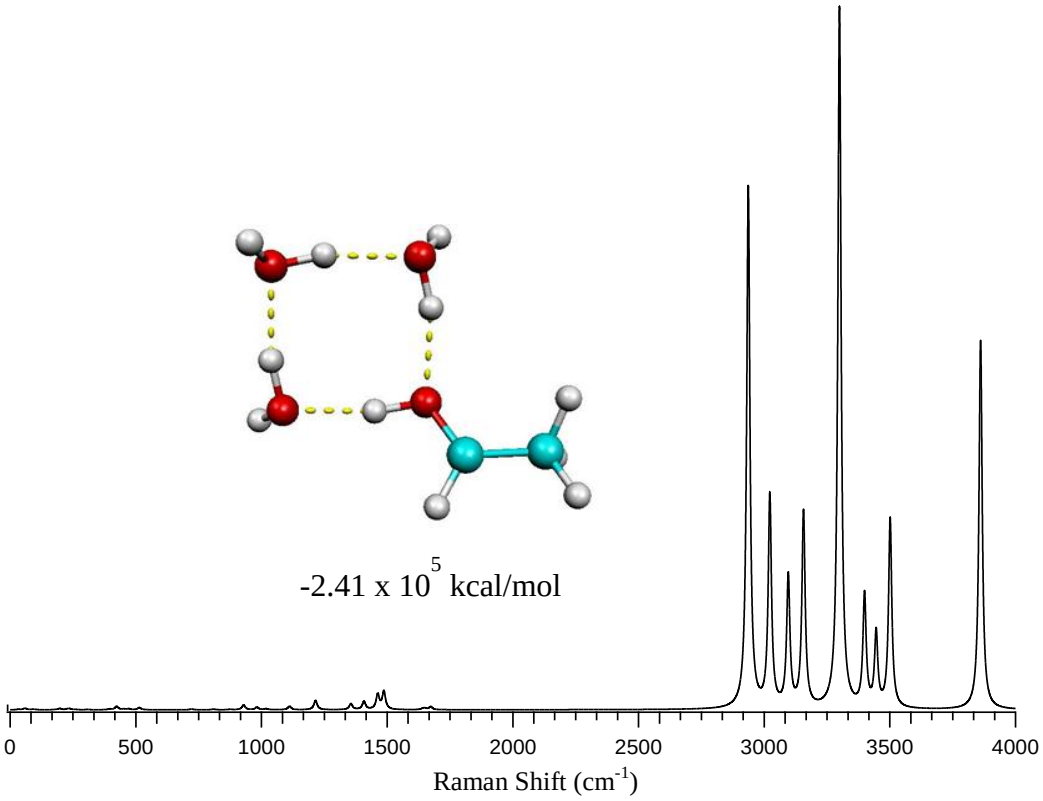

Figure 5.9: Simulated Raman spectra for the optimized lowest-energy structure of 1-Hydroxyethyl radical with three water molecules.

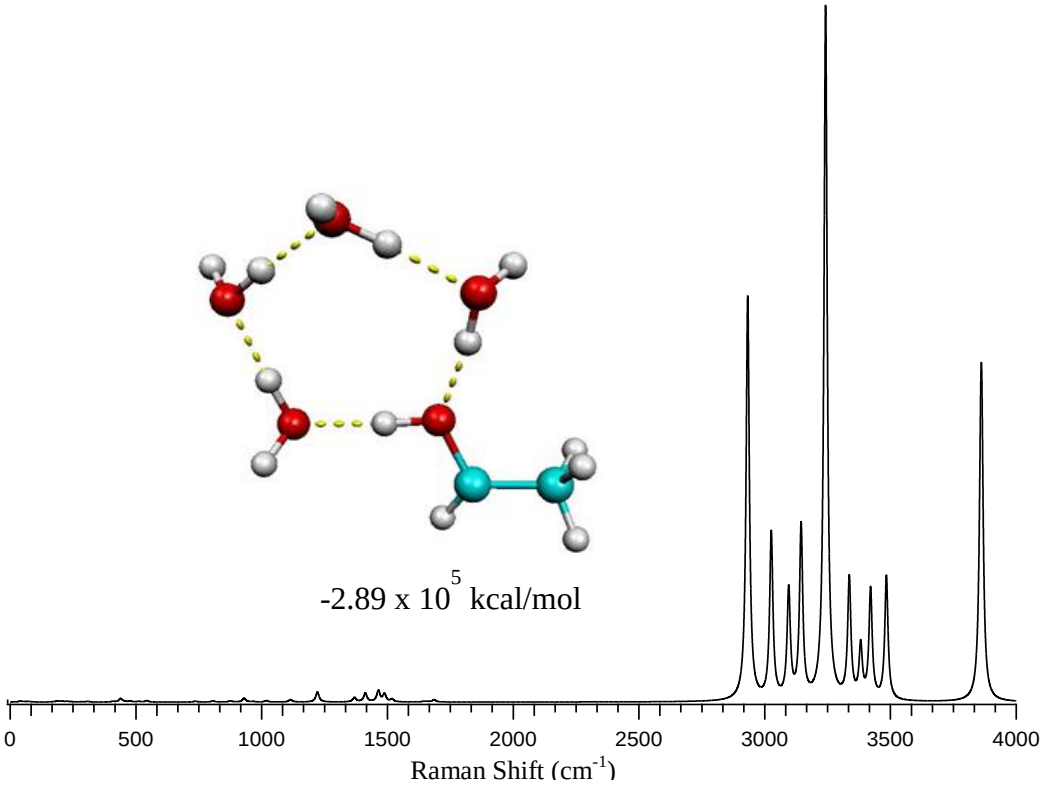

Figure 5.9.1: Simulated Raman spectra for the optimized lowest-energy structure of 1-Hydroxyethyl radical with four water molecules.

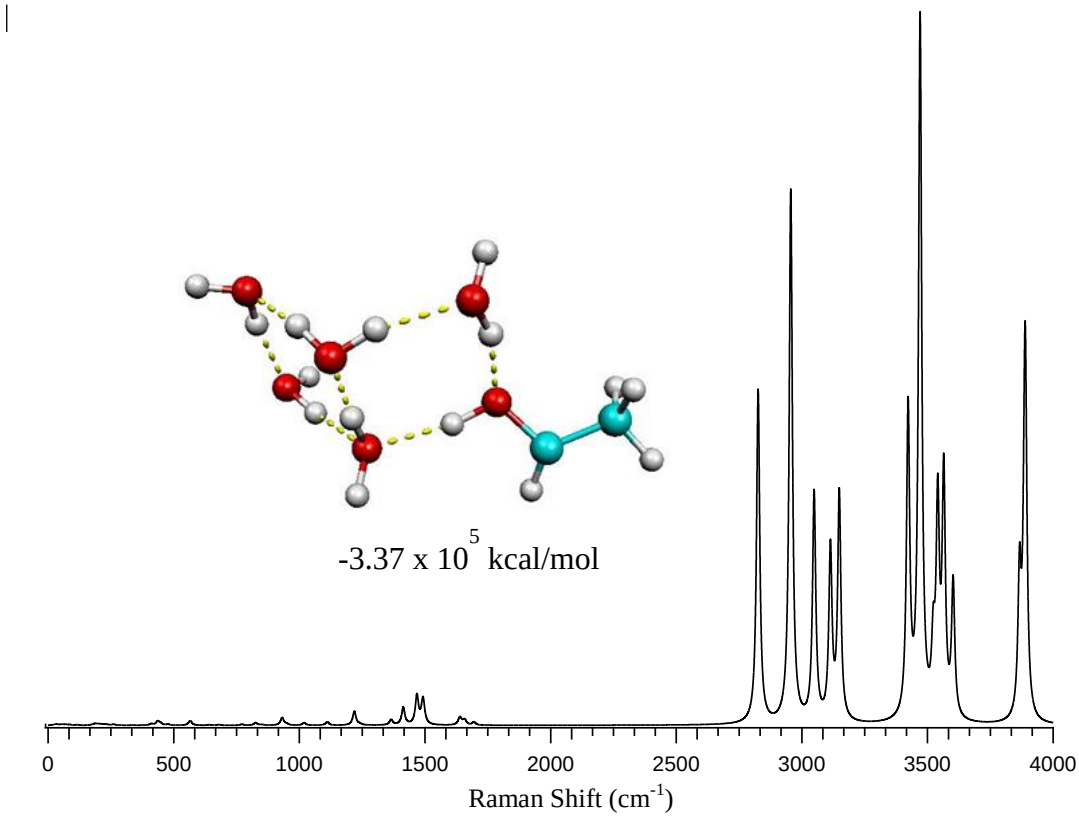

Figure 5.9.2: Simulated Raman spectra for the optimized lowest-energy structure of 1-Hydroxyethyl radical with five water molecules.

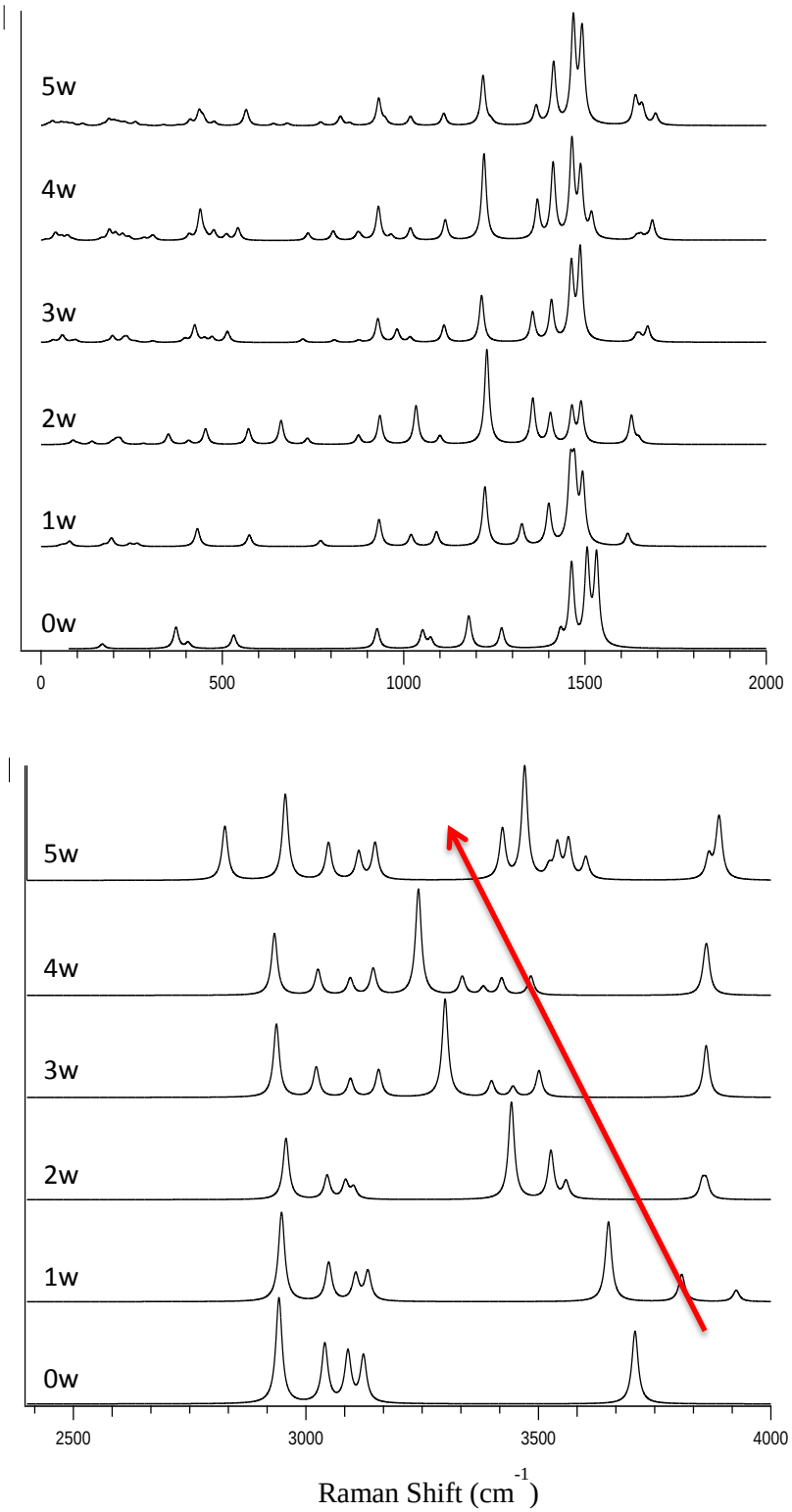

Figure 5.9.3: Spectra of all 6 lowest-energy structures superimposed on the same graph.

Vibrational Modes

Modes	0w[1HEO]	1w[B]	2w[B2]	3w[E3]	4w[G2]	5w[N2]
v1	3826.56	3630.8	3441.97	3299.38	3241.94	3422.71
v2	3138.94	3130.55	3102.72	3156.35	3144.68	3148.72
v3	3097.04	3091	3085.18	3095.7	3095.33	3113.54
v4	3035.55	3027.63	3045.63	3022.28	3025.99	3048.62
v5	2945.1	2932.55	2957.14	2936.55	2932.31	2955.7
v6	1487.59	1488.86	1490.94	1487.34	1518.25	1493.44
v7	1463.28	1468.66	1488.67	1486.37	1488.22	1490.5
v8	1444.3	1458.35	1463.94	1462.49	1464	1467.91
v9	1395.26	1399.44	1404.77	1407.61	1412.15	1413.52
v10	1269.45	1323.56	1356.19	1355.66	1368.84	1365.34
v11	1203.61	1219.28	1229.5	1215.01	1221.62	1218.96
v12	1057.35	1089.26	1100.17	1111.45	1114.68	1110.67
v13	1019.06	1018.89	1034.15	1017.83	1018.74	1018.83
v14	926.84	929.6	934.44	928.89	930.43	931.26
v15	537.79	535.69	572.14	513.84	542.97	563.24
v16	407.46	424.24	453.64	471.46	476.34	477.28
v17	356.19	244.53	407.12	423.73	439	435.98
v18	177.27	185.77	210.54	197.28	188.33	186.69

Table 4.2: Table comparing all of the vibrational modes for each of the 6 calculated lowest-energy structures.

Discussion

The lowest-energy structures found using the Gaussian09 program and the method and basis set detailed above (UB3LYP/aug-cc-pVTZ) are shown in Figures 4.2-5.8.5. 153 total structures were found, specifically 1 with no water molecules, 3 with one water, 9 with two waters, 18 with three waters, 37 with four waters, and 85 with five waters. It is important to remember that the unpaired electron in 1-Hydroxyethyl radical is located on the center carbon, so the increasing number of water molecules present in the system was expected to allow the delocalization of that negative charge, stabilizing the overall

molecule and lowering the energy of the structure. Observing the specific structures found, it is important to note that the hydrogen attached to the carbon containing the unpaired electron refrains from hydrogen bonding with water molecules due to electrostatic interactions preventing this bond. The lowest energy structure of each category (0 water molecules – 5 water molecules) was compared to analyze the change in energy and stabilization that occurs in increasing the solvation matrix. Using the formula 3N-6, it was determined that there should be a total of 18 vibrational modes. The vibrational modes of the lowest energy structures were found and can be seen in Table 4.2. In Figure 5.9.2, the simulated Raman spectra for the lowest-energy structures are compared. There are several unique peaks in the spectrum that correspond to specific vibrational motions that remain consistent, although shifted, in all of the lowest-energy structures for the radical in increasing solvation matrices. The vibrational mode, ν1, corresponds to the O-H stretching mode. There is a lone pair of electrons on the oxygen atom in the radical, so the lone pair and the unpaired electron on the center carbon repel each other, destabilizing the structure and aiding to its known reactivity. A red shift was observed in the peak corresponding to ν1, around 3500 cm^{-1}, as you increase the solvation matrices, going from 0 waters to 5 waters. This corresponds to the oxygen's negative charge being distributed into the water matrices. It is important to note that the 5 water calculations, and thus the simulated Raman spectra are still currently being run on the aug-cc-pVTZ basis set, so the data displayed is of the 6-31++G(*d*,*p*) basis set, and is therefore not as accurate. As you increase the solvation matrices, this delocalization of the negative charge on the center carbon was observed, so as would be expected, the red shift seen in the ν1, corresponds to that stabilization. Hopefully when the data taken for

the lowest-energy 5 water structure on the aug-cc-pVTZ basis set is compared to the rest of the data, the peak corresponding to ν1 will red shift in accordance.

Chapter 5: Conclusions and Future Works

Increased concentration of a byproduct of ethanol metabolism in the body, 1-Hydroxyethyl radical, has been correlated to cirrhosis of the liver and other alcohol-related illnesses. The ethanol-induced mutation of the enzyme cytochrome p450, specifically CYP2E1, is responsible for the production of this radical, and little is known about its hydrogen-bonded interactions with water molecules. The human body is composed of roughly 60% water, so the research done in this experiment could be used to map better drug delivery systems or for other pharmaceutical applications, and a better understanding of how this radical is interacting with water in nature is crucial for these purposes. The theoretical results found in this study show that increasing the solvation matrix with the radical decreases the overall energy and stabilizes the highly unstable and reactive radical.

Future work for this experiment is to get the matrix isolation Raman spectrometer into working condition so that experimental data can be compared to the computational data found. The experimental plan is to hit a solution of hydrogen peroxide and ethanol with radiation to produce the hydrogen peroxide radical. This radical will then be interacted with ethanol to produce 1-Hydroxyethyl radical and water. This reaction would take place on the gold plate inside the matrix chamber, and using cryotechnology, the final

products will be frozen down, warmed up slightly to react, and then frozen down again so that the radical can be analyzed by Raman spectroscopy. It is to be determined whether or not this reaction will be successful, but as of now this is current plan.

References:

1.Albano, E.; Tomasi, A.; Goria-Gatti, L.; Dianzani, M. U., Spin trapping of free radical species produced during the microsomal metabolism of ethanol. *Chemico-Biological Interactions* **1988,** *65* (3), 223-234.

2. Albanoa, E.; Clot, P.; Comoglio, A.; Dianzani, M. U.; Tomasi, A., Free radical activation of acetaldehyde and its role in protein alkylation. *FEBS Letters* 1994, *348* (1), 65-69.

3. Bahou, M.; Das, P.; Lee, Y. F.; Wu, Y. J.; Lee, Y. P., Infrared spectra of free radicals and protonated species produced in para-hydrogen matrices. *Physical Chemistry Chemical Physics* **2014,** *16* (6), 2200-2210.

4. Bernard, J.; Seidl, M.; Kohl, I.; Liedl, K. R.; Mayer, E.; Gálvez, Ó.; Grothe, H.; Loerting, T., Spectroscopic observation of matrix-isolated carbonic acid trapped from the gas phase. *Angewandte Chemie - International Edition* **2011,** *50* (8), 1939-1943.

5. Díaz Gómez, M. I.; Castro, G. D.; Delgado de Layo, A. M. A.; Costantini, M. H.; Castro, J. A., Cytochrome P450 reductase-mediated anaerobic biotransformation of ethanol to 1-hydroxyethyl-free radicals and acetaldehyde. *Toxicology* **2000,** *154* (1-3), 113-122.

6. "DFT." DFT. N.p., n.d. Web. 19 Mar. 2017.

7. Engel, Thomas, Philip Reid, and Warren Hehre. *Physical Chemistry*. Boston: Pearson, 2013. Print.

8. Feltham, E. J.; Almond, M. J.; Marston, G.; Wiltshire, K. S.; Goldberg, N., Reactions of hydroxyl radicals with alkenes in low-temperature matrices. *Spectrochimica Acta - Part A: Molecular and Biomolecular Spectroscopy* **2000,** *56* (13), 2589-2603.

9. Granger, Robert M., Hank M. Yochum, and Jill N. Granger. *Instrumental Analysis*. New York: Oxford UP, 2017. Print.

10. Karir, G.; Viswanathan, K. S., Phenylacetylene-water complex: Is it n···σ or H···π in the matrix? *Journal of Molecular Structure* **2016,** *1107*, 145-156.

11. Knecht, K. T.; Bradford, B. U.; Mason, R. P.; Thurman, R. G., In vivo formation of a free radical metabolite of ethanol. *Molecular Pharmacology* **1990,** *38* (1), 26-30.

12.McHale, Jeanne L. *Molecular Spectroscopy*. Boca Raton: CRC, 2017. Print.

13. Moore, D. R.; Reinke, L. A.; McCay, P. B., Metabolism of ethanol to 1-hydroxyethyl radicals in vivo: Detection with intravenous administration of α-(4-pyridyl-1-oxide)-N-t-butylnitrone. *Molecular Pharmacology* **1995,** *47* (6), 1224-1230.

14. Morzyk-Ociepa, B.; Nowak, M. J.; Michalska, D., Vibrational spectra of 1-methylthymine: Matrix isolation, solid state and theoretical studies. *Spectrochimica Acta - Part A: Molecular and Biomolecular Spectroscopy* **2004,** *60* (8-9), 2113-2123.

15. Navasumrit, P.; Ward, T. H.; Dodd, N. J. F.; O'Connor, P. J., Ethanol-induced free radicals and hepatic DNA strand breaks are prevented in vivo by antioxidants: Effects of acute and chronic ethanol exposure. *Carcinogenesis* **2000,** *21* (1), 93-99.

16. OpenStax. "Anatomy and Physiology." *2.2 Chemical Bonds | Anatomy and Physiology*. OpenStax, 06 Mar. 2013. Web. 05 Apr. 2017.

17. Tro, Nivaldo J. *Chemistry: A Molecular Approach*. 2nd ed. New Jersey: Pearson, 2011. Pearson. Web. 31 Mar. 2017.

18. Nordmann, R.; Ribière, C.; Rouach, H., Implication of free radical mechanisms in ethanol-induced cellular injury. *Free Radical Biology and Medicine* **1992,** *12* (3), 219-240.

19. Novak, R. F.; Woodcroft, K. J., The Alcohol-inducible form of Cytochrome P450 (CYP 2E1): Role in Toxicology and Regulation of Expression. *Archives of Pharmacal Research* **2000,** *23* (4), 267-282.

20. Ratliff, B. J.; Womack, C. C.; Tang, X. N.; Landau, W. M.; Butler, L. J.; Szpunar, D. E., Modeling the rovibrationally excited C2H4OH radicals from the photodissociation of 2-bromoethanol at 193 nm. *Journal of Physical Chemistry A* **2010,** *114* (14), 4934-4945.

21. Sherrill, C. David. "Basis Sets in Quantum Chemistry." *School of Chemistry and Biochemistry, Georgia Institute of Technology* (n.d.): n. pag. Georgia Institute of Technology. Web. 11 Apr. 2017.

22. Sosa, C.; Schlegel, H. B., An ab initio study of the reaction pathways for OH + C2H4 → HOCH2CH2 → products. *Journal of the American Chemical Society* **1987,** *109* (23), 7007-7015.

23. Stoyanovsky, D. A.; Wu, D.; Cederbaum, A. I., Interaction of 1-hydroxyethyl radical with glutathione, ascorbic acid and α-tocopherol. *Free Radical Biology and Medicine* **1998,** *24* (1), 132-138.

24. Wiltshire, K. S.; Almond, M. J.; Mitchell, P. C. H., Reactions of hydroxyl radicals with trichloroethene and tetrachloroethene in argon matrices at 12 K. *Physical Chemistry Chemical Physics* **2004,** *6* (1), 58-63.